5-1985

Analysis of a Rocket-Borne Resonant Scatter System for Measurement of Atomic Oxygen

Neil B. Myers
Utah State University

ANALYSIS OF A ROCKET-BORNE RESONANT SCATTER SYSTEM FOR MEASUREMENT OF ATOMIC OXYGEN

by

Neil B. Myers

A thesis submitted in partial fulfillment
of the requirements for the degree

of

MASTER OF SCIENCE

in

Physics

UTAH STATE UNIVERSITY
Logan, Utah

1985

ACKNOWLEDGMENTS

I would like to thank my committee, Kay D. Baker, L. Carl Howlett, and William Pendleton, for their numerous contributions to this project, Dr. Gordon Lind for his support as Department Chairman, and James Elwell for his work on developing most of the computer code. I would also like to thank Dr. Peter Banks for his role in bringing me to Utah State University.

Finally, I would like to extend my appreciation to my parents, Harry and Josephine Myers, and my step-father, Emanuel Eschwege, for their crucial role in providing me with the motivation and encouragement to pursue my career.

This work was supported by Air Force Geophysics Laboratories under contract number F19628-74-C-0130.

Neil Brubaker Myers

TABLE OF CONTENTS

LIST OF TABLES

LIST OF FIGURES

ABSTRACT

Analysis of a Rocket-Borne Resonant

Scatter System for Measurement

of Atomic Oxygen

by

Neil B. Myers, Master of Science

Utah State University, 1985

Major Professor: Dr. Kay D. Baker
Department: Physics

A computer model has been developed at Utah State University for interpreting the results of a rocket-borne resonant scatter measurement system using 1304 Å radiation. Atomic oxygen densities are obtained from 65 to 140 km from three rocket flights. The resolution of the system is < 0.1 km, and considerable structure has been observed. The variety of shapes exhibited by the three profiles suggest a dynamic nature to atomic oxygen density profiles in the lower ionosphere. Maximum densities between 2.6×10^{11} and 1.2×10^{12} cm^{-3} were observed at altitudes between 92 and 95 km.

(118 pages)

CHAPTER I

INTRODUCTION

The development of a method to measure atomic oxygen densities in the atmosphere over the peak density range with better resolution and accuracy than previously attained was undertaken at Utah State University (USU). The method chosen by USU was the resonant scatter method flown on a sounding rocket to provide a vertical profile of the atomic oxygen density between 65 and 140 km. Sounding rockets provide a vertical profile (with some horizontal component) over a very short period of time (three minutes). The resonant scatter method uses a lamp source to emit photons in a restricted frequency range in the region of 1304 Å. This corresponds to the energy difference for a resonant transition of atomic oxygen. A resonant transition is an allowed transition involving a two step process of absorption of a photon by an unexcited atom in the ground state, and the subsequent emission of a photon of almost the same frequency in a random direction. A detector for photons of the same frequency range as the lamp measures the number of photons scattered by the atmospheric atomic oxygen. A computer model has been developed to interpret the detector photon count into an atmospheric atomic oxygen density. This report is an analysis of the resonant scatter technique adopted by USU, and the computer model developed to interpret the data. The model is used to interpret the data from three rocket flights, and the results are compared with other measurements of atomic oxygen density to substantiate the validity of the technique.

Literature Review

The measurement of atomic oxygen densities remains an interesting and challenging problem in the upper atmosphere. This is due to the extremely reactive nature of atomic oxygen, and the low density of atomic oxygen compared to molecular oxygen and nitrogen below 110 km. A number of different methods for measuring atomic oxygen have been used in the past, providing information on different aspects of the atomic oxygen density profile, but none are without limitations. For example, satellites orbiting mass spectrometers usually provide information from above 110 km while satellites measuring slant column oxygen emissions can cover the altitude range of about 80 km to 120 km. Since every 90 minutes or so a satellite completes one orbit and returns to approximately the same place, changes on a time scale of 90 minutes can be measured. They also cover a wide region of latitude. Hence satellite measurement systems can easily measure temporal and latitudinal changes, but do not have very good resolution at the oxygen peak density altitude (approximately 95 km). Rocket-borne systems can have better resolution at the peak density altitude (being in situ), but individually do not measure temporal or latitudinal variations. All measurement systems seem to have the common problem of determining absolute values of densities of atomic oxygen.

The different methods of measuring atomic oxygen provide a means of comparing results, which helps in determining confidence in any or all of the measurement techniques. The various techniques include mass spectrometer measurements, both rocket-borne and on satellites, rocket-borne silver film measurements, chemical releases, satellite drag measurements, 5577 Å rocket-borne photometers, satellite slant

column measurements, rocket-borne catalytic probes, and the 1304 Å resonant scatter technique.

Mass spectrometers have been used on both rockets [Pokhunkov, 1972] and satellites [Hedin et al., 1977]. The problems of mass spectrometers in measuring atomic oxygen include reactions with the wall, and with gas molecules within the instrument [von Zahn, 1967]. The controversy over mass spectrometers is to what degree losses to the walls occur, and disagreement over the proper correction factor has been a common problem [Nier et al., 1976]. It has been suggested [Lake and Nier, 1973] that mass spectrometers measure atomic oxygen densities a factor of 2.5 low due to losses of oxygen atoms reacting with the walls on impact. But exposure to oxygen during flight could result in a surface conditioning that could lessen this factor at later times in the flight [Philbrick et al., 1974]. Thus the consistancy of these results must remain questionable. In a review paper [von Zahn, 1970] rocket-borne mass spectrometer results have been rejected by von Zahn in favor of satellite drag-derived mass densities.

Supercooled mass spectrometers have been flown to minimize these problems [Offermann and Trinks, 1971]. Using a cryoion source extends the altitude range of rocket-borne mass spectrometers down to below 85 km [Scholz and Offermann, 1974]. Resolution of less than 2.5 km is still a problem, along with absolute calibration. Trinks and others used a calibration procedure that multiplies the sensitivity of the methane positive ion by the ratio of the ionization cross sections of O plus and methane positive ions. This is obviously an indirect method of calibration, and a 25% probable error has been reported [Trinks

et al., 1978]. In the past, supercooled mass spectrometers have provided the most reliable measurements of atomic oxygen densities. However the complexity of the system increases the cost, and the difficulty of making the measurement. Recombination of oxygen atoms within the instrument is still an unknown factor. Since oxygen atoms must be brought within the instrument, the measurement time is slow. Hence the time/spatial resolution is still not good enough for measuring small structure in the density profile.

Mass spectrometers on satellites have the advantage of repeated measurements from close to the same location over time. A vertical altitude profile is not provided and satellite mass spectrometers do not measure the peak density region. However wave-like structure and seasonal variations have been reported using this method [Reber et al., 1975].

Silver films have been employed to measure atomic oxygen [Henderson, 1974]. The problems of the technique include the consistancy of the film, and the differentiation of the integrated change of resistance. The surface recombination coefficient depends on the oxide thickness as well as the flux to the instrument [Thomas and Baker, 1972]. Resolution of the instrument therefore suffers. Henderson reported a standard deviation of 50%. Dickinson has used silver strips in conjunction with resonant scatter and mass spectrometer measurements [Dickinson et al., 1980], and reported that the silver strip technique was not consistant enough to be recommended.

The rocket-borne measurement of the 5577 Å airglow allows indirect calculation of atomic oxygen densities [Offermann and Drescher, 1973]. The problems of this measurement technique [Donahue and Guen-

ther, 1975] include assumptions of emission and quenching processes, and associated rate constants. Accuracy and resolution suffer as a result of the spatial differentiation of an integrated airglow emission. A rocket flight with both a mass spectrometer and a 5577 green line photometer has been flown [Philbrick et al., 1974]. The 5577 A photometer measurement system predicted a substantially different profile than the mass spectrometer measured.

Satellite drag has obvious problems in determining density [Imbro et al., 1975], including the shape of the satellite. Imbro points out that in situ measurements of drag have been made as by-products of satellites and rockets designed for other use. The lack of precise knowledge of the dependence of aerodynamic coefficients on altitude and other parameters in the satellite environment limit this technique. Again however, satellite drag measurements have provided interesting seasonal and latitudinal variations not easily duplicated by rocket-borne instrumentation [Forbes and Marcos, 1980].

Satellite slant column emission has been used with the 5577 A radiation [Wasser and Donahue, 1979] with worse resolution limitations than encountered with the rocket-borne 5577 A measurement. This is because of the integration of the emission over a very large slant range. Figure 1 [Donahue et al., 1973] shows the technique of slant column emission measurements. The need for knowledge of excitation and quenching mechanisms, and rate constants provide obvious limitations. Attitude uncertainty of the satellite causes an altitude uncertainty of + 4 km, and hence peak density altitudes are not accurate by satellite slant column emission measurements [Offermann and Drescher, 1975]. The temperature dependence of rate coefficients also

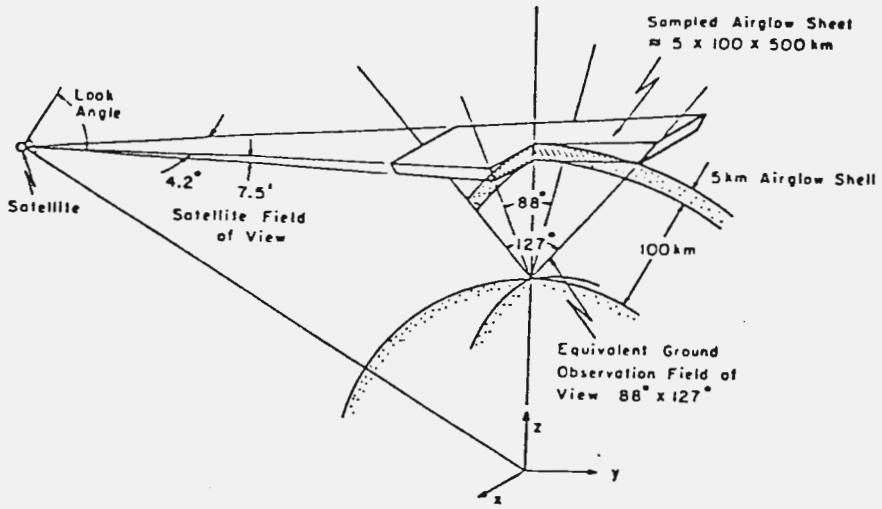

Figure 1. Geometry of the slant column emission measurement. From Donahue et al., [1973].

limits this technique. Seasonal and latitudinal variations however are easily measured with the slant column emissions [Donahue et al., 1973].

The chemical release of nitric oxide has been used to measure atomic oxygen densities in the 90 km to 160 km region [Golomb and Good, 1972]. The knowledge of the chemiluminous rate constant and the definition of the reaction volume limit this technique. The absolute accuracy of this technique is uncertain [von Zahn, 1970].

Resonant Scatter Technique

To avoid these problems, a method was sought to give reliable measurements over the peak density region with better resolution and accuracy than previously attained. To this end, a resonant scatter technique has been developed at USU for sounding rocket use. The

resonant scatter technique uses the excitation and emission of radiation of a particular wavelength of oxygen atoms to determine density. This allows measurement of atomic oxygen densities with minimal disturbance of the oxygen atoms. Since resonant scattering involves radiation propagation, the measurements are made with very great speed. Hence this technique provides excellent resolution of less than a tenth of a km. However the random scatter of the data caused by background 1304 Å airglow at altitudes above 120 km [Meier and Lee, 1982; Strickland and Donahue, 1970] degrades the measurements above this altitude.

The resonant scattering technique uses an oxygen resonant lamp which produces radiation of three wavelengths. They are 130.217 nanometers (nm), 130.487 nm, and 130.604 nm, and are in the ultra-violet region. This triplet is then resonantly scattered from the atmosphere by atomic oxygen and Rayleigh scattered by major species. The Rayleigh scattering is a much smaller effect and is overwhelmed by the oxygen resonant scattering [Howlett and Baker, 1977]. A detector sensitive to these wavelengths records the returned signal.

The two methods of interpreting the data are by either direct calibration, or by computer modeling of a transfer function. The calibration process is extremely difficult, due to the reactive nature of atomic oxygen. Therefore a system which flows a constant density of atomic oxygen by the detector is neccessary [Dickinson et al., 1980]. Actually Dickinson has calibrated an absorption measurement system and flies the absorption experiment on the same rocket as the resonant fluorescence experiment. The resonant fluorescence measurement is

then calibrated from the absorption experiment. The absorption technique is not reliable for low densities, so an extrapolation must be used in the calibration. For these reasons USU has developed a computer model for interpreting the data returned from the resonant lamp system. The computer model is described and is used to interpret data from three rocket flights, producing atomic oxygen density profiles for the three flights. The rockets used were a Nike-Orion launched from Red Lake, Ontario, Canada during the February 26, 1979 eclipse; a Taurus-Orion launched from Andoya, Norway November 16, 1980; and a Taurus-Orion launched from Wallops Island, Virginia on June 29, 1982.

CHAPTER II

MEASUREMENT USING RESONANT TRANSITION

Resonant Scattering

To create a computer model for interpreting the rocket flight resonant scatter measurement of atomic oxygen, a basic understanding of the 130 nm radiation propagation through a medium containing oxygen atoms is necessary. First consider a parallel beam of continuous spectrum radiation of constant intensity entering a region containing atomic oxygen. As the radiation encounters an oxygen atom, there is a certain probability that one photon will be absorbed by the atom causing a transition from state 1 (ground state) to an excited state. For an atom in the excited state, there is a certain probability for spontaneous emission in a random direction, returning to the ground state after a finite lifetime. This two step process is known as resonant scattering. There is also a certain probability for an atom in the excited state to undergo a transition from the excited state to state 1 when exposed to isotropic radiation, emitting one photon in the same direction and in phase with the stimulating photon (stimulated emission).

Since the velocity distribution of a group of atoms is normally expected to be Maxwellian, the most probable velocity of any atom is zero, assuming no bulk motion. Then the photon most likely to be absorbed is one whose frequency corresponds to the energy level difference of the transition. This frequency is called the line center (ν_0). For an atom with a non-zero velocity, the frequency of photons it can absorb is shifted from the line center due to the

doppler shift of light. As the radiation propagates further into the medium, the number of atoms encountered increases, and the number of photons absorbed increases. Since the percentage of photons absorbed is greatest for frequencies at the line center, the continuous spectrum propagating through the medium exhibits decreased intensity at the line center (Figure 2, from Mitchell and Zemansky [1961]).

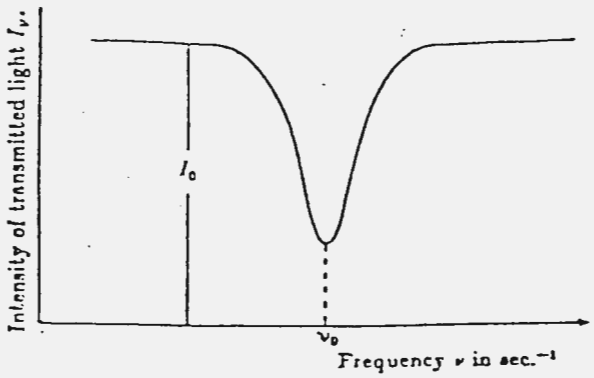

Figure 2. An absorption line. From Mitchell and Zemansky [1961].

The absorption (or emission) frequency shape due to the doppler shift of light caused by the random thermal motion of the absorbing (or emitting) atoms is referred to as a doppler profile. For the case of oxygen atoms, the ground state is a triplet, and there are three absorption lines at the three line centers corresponding to the three transition energy differences.

To excite the resonance transitions in atomic oxygen in the atmosphere a lamp using atomic oxygen emissions is used by USU. The transitions involved in the oxygen resonance radiation use a triplet at the ground state $(2p)^4\ {}^3P_J$ energy levels with J = 0, 1, and 2. As the atomic oxygen in the lamp is excited, one of the 2p electrons

makes the transition to level $2p^3(^4S^0)3s^1\ ^3S^0$ which corresponds to a wave number of 76,795 cm^{-1}. When the electron returns to the ground state, it returns to one of the J levels according to the statistical weights of 1, 3, and 5. These weights are for the J = 0, 1, and 2 levels respectively. This is of course for the ideal situation in which the 130.604 nm radiation would have a relative intensity of 1, compared to the 130.487 nm radiation with relative intensity of 3, and 130.217 nm radiation with relative intensity of 5 [Howlett and Baker, 1977].

Line Broadening

For the ideal situation of atomic oxygen resonant scattering, the emitting atoms radiate at three and only three specific frequencies, and the absorbing atoms absorb these same three and only these three frequencies. In reality, a small range of frequencies is emitted surrounding each of the singular frequencies, creating a frequency emission profile. In general, the intensity of emission decreases as the frequency separation away from the ideal emission frequency increases. Similarly, a range of frequencies is absorbed by the oxygen atoms creating an absorption profile. Again, the intensity of absorption decreases as the frequency separation away from the ideal absorption frequency increases. To determine the shape of the emission and absorption profiles, one must examine the cause of the frequency broadening.

There are five processes in general that contribute to the broadening of the emission and absorption profiles. They are 1) natural broadening due to the finite lifetime of the excited state, 2) doppler

effect broadening due to the thermal motion of the atom, 3) Lorentz broadening due to collisions of the atom with foreign gases, 4) Holtsmark broadening caused by collisions of the atom with other absorbing atoms of the same kind, and 5) Stark effect broadening due to collisons of the atom with electrons and ions. Both Lorentz and Holtsmark broadening are refered to as pressure broadening. They both have the effect of broadening the line profile, shifting the maximum of the profile, and changing the shape to an asymmetrical one. With the foreign gas pressure below 5 Torr the contribution of Lorentz broadening is small compared to doppler broadening [Mitchell and Zemansky, 1961, p. 98]. Stark effect and Holtsmark broadening are not too large if the gas is not electrically excited and its pressure is kept below 0.01 Torr. With the uncertainty of the lamp operating conditions, ignoring these processes can not be done with confidence. An empirical expression which takes into account the pressure broadening in the lamp is developed in the next chapter. Doppler broadening is large in comparison with the very narrow natural width. This natural width is replaced with a doppler broadened Gaussian half width due to the kinetic energy of the emitting atoms, and takes the following form [Strickland and Donahue, 1970]

$$\Delta\nu_d = \lambda_0^{-1}(2kT/m)^{.5} \qquad (1)$$

where $\Delta\nu_d$ = doppler half width frequency

λ_0 = line center wavelength

k = Boltzmann's constant

T = temperature

m = mass of atom

The doppler half width would be about 0.0004 nm at a temperature of 900 Kelvin.

For maximum absorption of the emitted radiation the absorbing atoms should have line profiles identical to the emitting atoms. This basically means the emitting atom temperature should be equal to the absorbing atom temperature. This is not the case however, since the emitter temperature (assumed to be 900 Kelvin, but could vary quite a bit) is greater than the absorber temperature (usually 200 to 500 Kelvin). With the absorbing temperature less than the emitting temperature, the absorbing line profile is thiner than the emitting line profile as shown in Figure 3 from Howlett and Baker [1977], which shows the emission and absorption profiles normalized at their peak intensities.

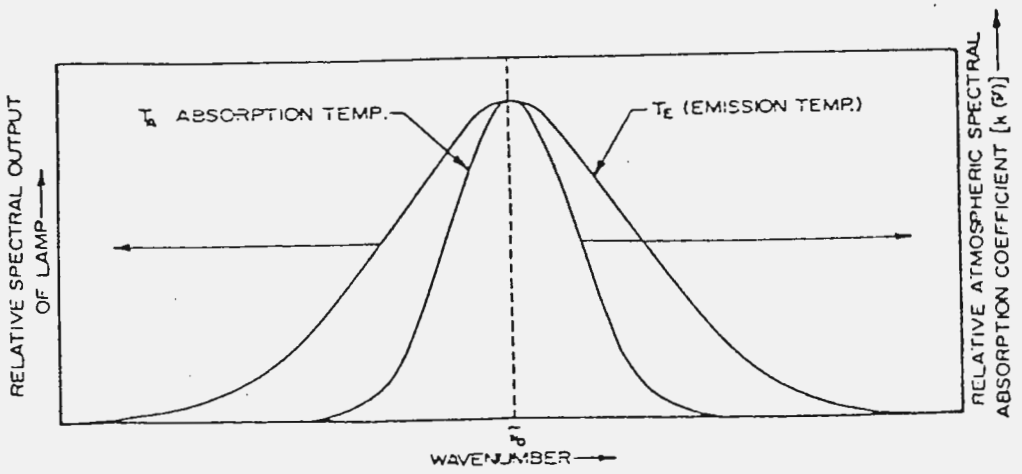

Figure 3. Doppler line profiles of different temperature.
From Howlett and Baker [1977].

This causes the emitting line profile to be preferentially absorbed at the line center, causing self-reversal as the radiation penetrates

farther into the absorbing medium. Self-reversal also occurs in the lamp itself, since there are oxygen atoms in the ground state in the lamp. It is this self-reversal which limits the atomic oxygen density we can use in the lamp. The self-reversal of the emitting line profile causes the ideal 5:3:1 relative intensity ratio to change. A profile of 4.3:2.7:1 is the actual relative intensity ratio measured and used in the computer model.

Measurement Technique

The lamp used by USU consists of an RF excited low pressure discharge in an open flow system of helium and oxygen. The lamp was developed by Professor Carl Howlett and co-workers at USU. The oxygen-helium mixture released into the chamber is controlled by a pressure valve. This mixture flows into a coaxial cavity with a center electrode. A high voltage RF exciter produces a discharge which dissociates the molecular oxygen and excites the atomic oxygen resonance lines. A window which has a short wavelength cutoff of approximately 125.0 nm is used at the end of the coaxial chamber. This window is carefully controlled to be opaque to Lyman-alpha radiation but transparent to the resonance radiation. The system uses a dynamic equilibrium with oxygen flowing through the coaxial discharge chamber at a constant and controllable partial pressure. Although the lamp hopefully operates in an equilibrium condition, there is a transient condition that exists upon beginning the process. The exact behavior of lamp intensity does not seem to be consistent from lamp to lamp. Because of this, a lamp intensity monitor is included in the hardware to measure the lamp intenstiy during the rocket flight. This

information is used when reducing the data to determine an oxygen density in the atmosphere.

The lamp intensity monitor consists of a nitric oxide filled ionization chamber at 200 Torr pressure. The ionization potential of the nitric oxide and a calcium fluoride window provide upper and lower wavelength cutoffs. So the 1304 and 1356 Å emissions are the only dominant wavelengths to which the detector is sensitive. The 1356 Å emissions are much less intense than the 1304 Å emissions. A probe in the ionization chamber detects the amount of ionization occuring in the monitor, and hence lamp operating conditions.

The detector used in the measurement of the atomic oxygen resonantly scattered radiation is an EMR 541 G photomultiplier. Magnesium fluoride is used as a window material to provide selective wavelength response, particualarly in rejecting 121.6 nm Lyman-alpha radiation. In addition to the window, interference filters are used to further eliminate unwanted wavelength response. This of course is done at the expense of sensitivity.

To measure atomic oxygen densities in the upper atmosphere using the 1304 Å resonant scatter technique, a light source (oxygen lamp) is installed on a sounding rocket. A detector is mounted and aligned so that the detector axis of view intersects the source. The general configuration of the payload is shown in Figure 4.

The instruments are located behind a door in the rocket skin. The door protects the instruments from overheating when the rocket travels through the dense lower atmosphere.

Sounding rockets travel at supersonic speeds (on the order of 1 km per second) and are capable of reaching altitudes of 140 km or

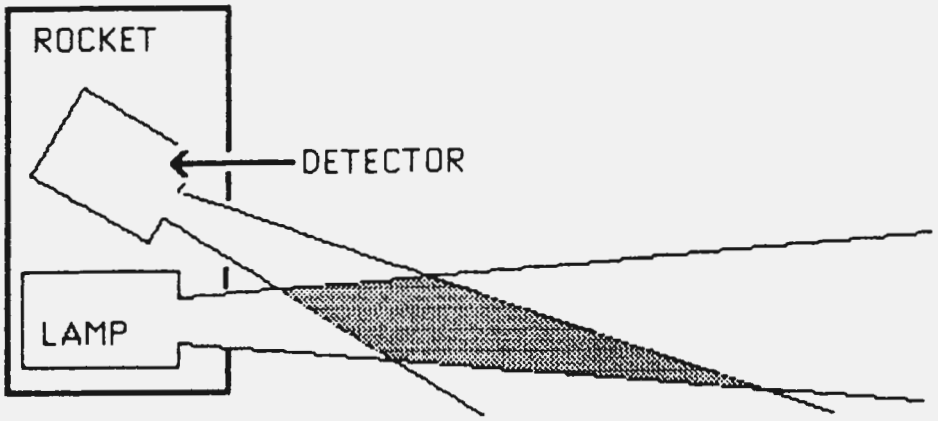

Figure 4. Resonant scatter instrument configuration.

more. They usually are spin stabalized, with typical spin rates of 7 or 8 Hertz. After the rocket has been launched and leaves the dense lower atmosphere, the door is ejected (usually at approximately 65 km) to allow both instruments to view the atmosphere. Baffles in front of the source and detector clearly define solid cones of view. The configuration (Figure 4) is designed to place the volume of intersection of the two solid cones just outside the rocket skin (usually a few centimeters). Since the rocket velocity is predominantly vertical, the instruments are mounted so as to view horizontally. This minimizes the doppler effect on the emitted radiation due to the rocket motion. For a horizontal rocket velocity of 300 meters/second (m/sec), a doppler shift of 0.00013 nm occurs for the 130.4 nm radiation. Horizontal velocities of 500 m/sec cause a 0.0002 nm doppler shift. Since the half width of the lamp emission lines should be between 0.0004 and 0.001 nm, the horizontal velocity of the rocket

should not have a major effect. With the supersonic speeds of sounding rockets, this doppler effect could reduce the resonant scattering if a significant portion of the rocket velocity were along the emitted beam direction. For a velocity of 1 km/sec (typical rocket velocity), a doppler shift of 0.00043 nm, comparable to the normal half width, would occur. This would shift a portion of the emission profile out of the absorption profile frequency range, and decrease the number of resonant transitions occuring.

The source is repeatedly turned on and off for equal amounts of time (0.016 for the first two flights described herin, 0.020 seconds for the third flight). With the source on, radiation near 1304 Å is emitted into the atmosphere. Since atoms (and molecules) other than oxygen are also present, they may compete with the oxygen atoms for the 130 nm radiation. The competing processes include Rayleigh scattering from major species and photoabsorption by O_2, O_3, CO_2, and N_2.

The amount of radiation Rayleigh scattered depends on the total density of the atmosphere ([M]) and the cross section (σ_r) for the process. The product of cross section times density yields the percentage of incident radiation per unit length which will partake in the process considered. This product is very useful in comparing the importance of different processes occuring in the atmosphere. At an altitude of 70 km with an atmospheric density of 10^{15} cm^{-3} with σ_r equal to approximately 3.5×10^{-24} cm^2 for 130.4 nm [Penndorf, 1957], the product $\sigma_r[M]$ is approximately 10^{-9} cm^{-1}. At 70 km the density of oxygen atoms ([O]) is about 10^9 cm^{-3}, and the 130.4 nm cross section for oxygen atoms (σ_o) is about 2.1×10^{-13} cm^2. So the product $\sigma_o[O]$

for oxygen resonance is about 10^{-4} cm^{-1}. So the Rayleigh scattering is about five orders of magnitude less important than the resonant scattering (at 70 km). Since the total density decreases with altitude and the atomic oxygen density increases with altitude (until 95 km), the Rayleigh scattering becomes even less important at higher altitudes. At 110 km the product of cross section times density for Rayleigh scattering decreases to about 10^{-11} cm^{-1}. The cross section for ozone photodissociation is 10^{-17} cm^2 [Hudson, 1971; Tanaka et al., 1953]. For altitudes of 70 and 80 km (densities of 10^9 and 10^8 cm^{-3} respectively) this yields products of 10^{-8} and 10^{-9} cm^{-1} respectively. This is again four or five orders of magnitude less important than the resonant scattering. The cross section to 130 nm radiation for NO is around 2×10^{-18} cm^2 [Watanabe et al., 1967], but because of the low density of NO (10^7 cm^{-3} at 90 km) the product $\sigma_{NO}[NO]$ is on the order of 10^{-10} cm^{-1}, very small compared to the other competing processes. Nitrogen is the most abundant species at 100 km with a density of about 10^{13} cm^{-3}, but because the cross section of N_2 is about 10^{-21} cm^2 [Watanabe and Marmo, 1956], it is ignorable in comparison to the oxygen resonant scattering. The cross section of CO_2 is about 10^{-18} cm^2 [McEwan and Phillips, 1975], and since the density is comparable to that of atomic oxygen, the photoabsorption of 130 nm radiation by CO_2 is ignorable compared to the oxygen resonance. Because of the large density of molecular oxygen (4×10^{14} cm^{-3} at 70 km) and the cross section of O_2 to 130 nm radiation being about 5×10^{-19} cm^2 [Lee, 1955], the product of cross section and density yields 2×10^{-4} cm^{-1}, which is about one third of the product for the resonant scattering at that altitude. This indicates that O_2 absorption does

have an effect on the return of the 130 nm radiation at densities of 70 km and below. The 130 nm radiation photodissociates oxygen molecules, creating two oxygen atoms for each molecule dissociated. For the 130 nm radiation, the dissociation leaves one atom in the ground state and one atom in the excited (^1S) state. Although a photon is lost in the process, an oxygen atom in the ground state is gained, which is then capable of resonantly scattering the 130 nm radiation. Hence the effect of the O_2 photoabsorption is unclear below 70 km. At larger altitudes, it becomes much less important than the resonant scattering process and can be ignored. Table 1 shows the product of cross section to 130 nm radiation times density for the major species in the atmosphere over the altitude region of interest.

TABLE 1. Cross Section Times Density for Major Species

Altitude (km)	$\sigma_0[O]$	$\sigma_{O_2}[O_2]$	$\sigma_{O_3}[O_3]$	$\sigma_{NO}[NO]$	$\sigma_{CO_2}[CO_2]$	$\sigma_{N_2}[N_2]$
70	6×10^{-4}	2×10^{-4}	7×10^{-9}	4×10^{-11}	1×10^{-6}	
80	2×10^{-3}	5×10^{-5}	7×10^{-10}	1×10^{-10}	1×10^{-7}	4×10^{-7}
90	2×10^{-2}	5×10^{-6}	2×10^{-10}	1×10^{-10}	2×10^{-8}	7×10^{-8}
100	6×10^{-2}	1×10^{-6}		1×10^{-10}	5×10^{-9}	1×10^{-8}
110	8×10^{-3}	2×10^{-7}		4×10^{-11}		

The major effect of the 130.4 nm radiation emitted by the lamp into the atmosphere is to resonantly excite oxygen atoms which then emit radiation in the same wavelength region. Some of this radiation reaches the detector and is measured. The detector measures radiation

not blocked by filters within its field of view. Electronics separate the measured counts made with the source on from the lamp off counts.

Eventually the off counts are subtracted from the on counts to remove any background signal. Figure 5 is an example of the measured 1304 Å background airglow from Fastie et al. [1964]. As the rocket travels upward through the atmosphere, an altitude profile of the count rate is obtained. A computer model translates this count rate into an atomic oxygen density profile. The profile is a vertical profile, with the addition of a small horizontal component associated with the rocket trajectory.

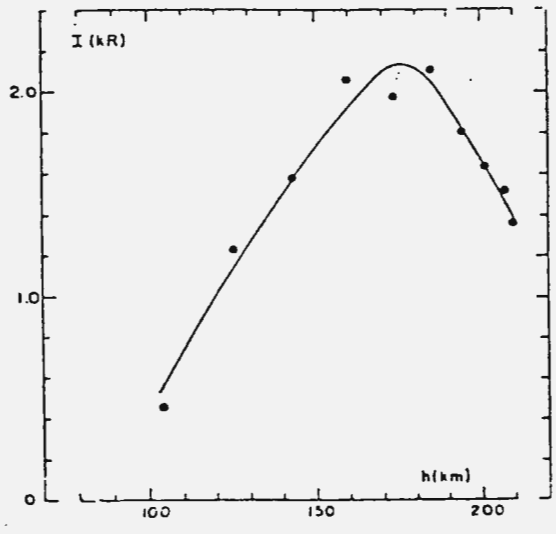

Figure 5. Measured 1304 angstrom airglow. From Fastie et al., [1964].

CHAPTER III

DERIVATION OF TRANSFER FUNCTION

The computer model developed at USU consists of two major sections. The first section creates a transfer function for atomic oxygen densities as a function of a count rate of photons predicted to return to the detector. This part of the model includes eight programs which use information about the physical properties of the resonance lamp and detector system. The results of this section can be used for any rocket flying the same instrument configuration. The second section of the model uses the rocket data as input to the previously derived transfer function for calculating atomic oxygen densities. This second section also provides for reducing the data using various averaging techniques.

To create a transfer function, one assumes the oxygen density and both emission and absorption temperatures are known. Given the density and temperature, attenuation of a signal propagating through the medium is calculated as a function of depth of penetration. Actually instead of depth of penetration, optical depth is used, which increases with distance into the medium. The cross section of oxygen atoms has to be modified to account for self-reversal in the transmitted signal. The self-reversal occurs because of the preferential absorption of the line center compared to the wings of the frequency profile. Because of this a normalized emission-absorption profile overlap function is calculated (or, an "effective microscopic cross section") as a function of optical depth. Using measurements of the field of view of the source-detector system, the calculation of light

emitted from the source and returned to the detector by first and second order resonant scattering is performed for the assumed oxygen medium density and temperature. Then the whole process is repeated increasing the assumed oxygen density in steps covering the expected atmospheric density range (10^7 to 10^{13} atoms per cubic cm). This is done for each temperature in steps between the expected temperature range (200 to 1000 Kelvin).

Attenuation

In the first section of the model, eight programs perform the separate tasks neccessary for creating a transfer function. The first program is named ATTEN. ATTEN calculates the normalized transmission of light as a function of optical depth, with the absorbing medium temperature as a parameter. For a very thin emitting layer with minimum lamp self-reversal an empirical expression for the emitted frequency distribution which approximately includes the line broadening resulting from the vapor pressure and temperature conditions in the lamp is [Mitchell and Zemansky, 1961, equation 60]

$$E(\nu) = C_0 \exp[-(\omega^2/\alpha^2)] \qquad (2)$$

where ν = frequency

C_0 = maximum intensity constant

$\omega = 2(\nu-\nu_0)/\Delta\nu_d(1n2)^{.5}$

ν_0 = line center frequency

$\Delta\nu_d$ = doppler half width

α = emission to absorption temperature ratio

This departs from a pure doppler line shape of

$$E(\nu) = C_0 \exp(-\omega^2) \tag{3}$$

The absorption of each of the three line centers of the signal due to oxygen atoms (assuming that there is no overlap of the three line profiles) is given by [Mitchell and Zemansky, 1961, equation 55]

$$A = \frac{\int E(\nu)\{1 - \exp[-k(\nu)l]\}d\nu}{\int E(\nu)d\nu} \tag{4}$$

For a pure doppler line [Mitchell and Zemansky, 1961, p. 103]

$$k(\nu) = k_0 \exp(-\omega^2) \tag{5}$$

where k_0 = absorption coefficient

l = length of propagation into medium

$k_0 l$ = optical depth

Using the empirical expression for the emitted frequency distribution the transmission of the signal becomes

$$T = \frac{\int \exp[-\omega^2/\alpha^2 - (k_0 l)\exp(-\omega^2)]d\omega}{\int \exp(-\omega^2/\alpha^2)d\omega} \tag{6}$$

The transmission of the signal is calculated using assumed optical depths from 0.0 to 19.5 in increments of 0.5. At the line center very little radiation penetrates through to an optical depth of 19, so calculations for larger optical depths would add little. The program PATTEN plots transmission versus optical depth. This is done for each

temperature of 200, 300 K, up to 1000 K. Figure 6 shows the plot for absorber temperature equal to 300 K.

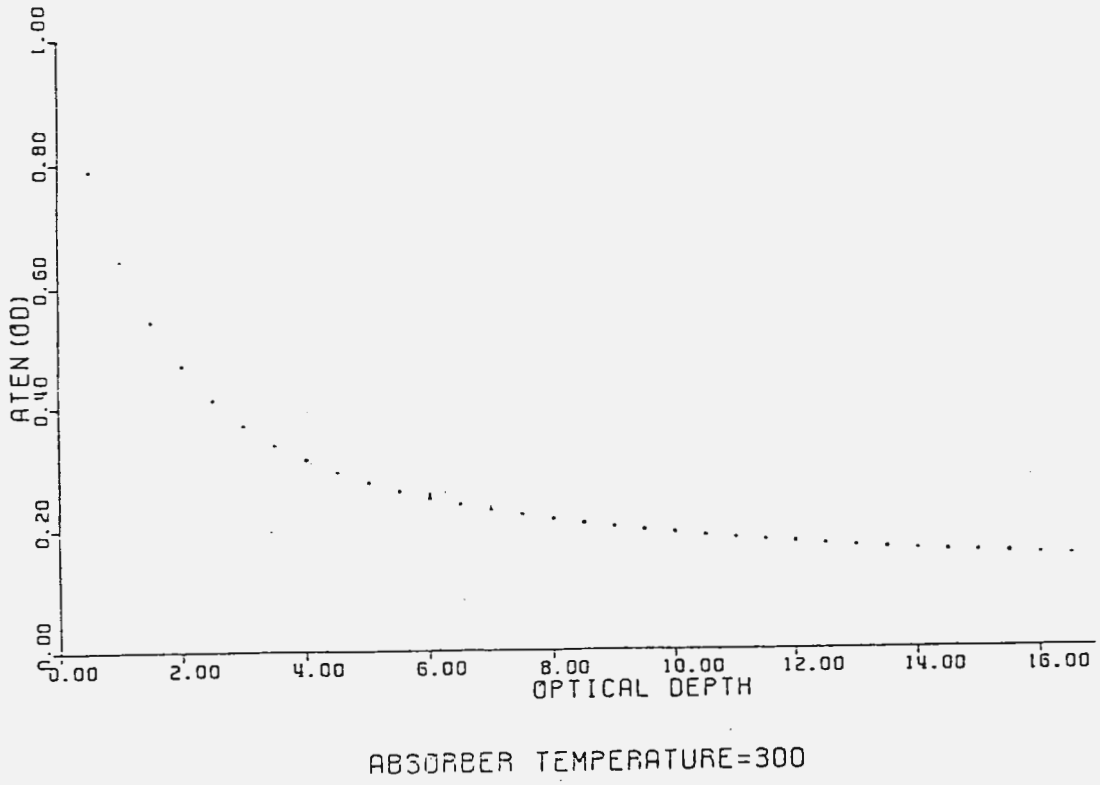

Figure 6. Normalized transmission.

Cross Section

The next program is named SIGMA. SIGMA calculates the effective microscopic cross section of atomic oxygen as a function of optical depth, with the absorbing medium temperature as a parameter. As a signal propagates through the medium, the line center is preferentially absorbed. This is because the absorption frequency profile is a pure doppler profile, but usually thinner than the doppler width of the emitted radiation of the lamp. This is due to the normally larger temperature of the lamp compared to the absorbing oxygen medium tem-

perature. This alters the emitted line profile shape from that of a pure doppler profile to one that has been self-reversed. A severely self-reversed profile has a double hump structure with a minimum at the line center. This occurs at large optical depths.

An attempt to include the effects of self-reversal on the cross section of oxygen atoms to the 1304 Å triplet radiation was made in the form of an equation representing a normalized overlap factor. The absorption frequency profile is pure doppler, while the transmitted signal reaching the absorbing atom has become self-reversed. The overlap of the doppler absorption profile with the self-reversed profile is represented by

$$\sigma = \frac{\int \exp[-\omega^2/\alpha^2 - (k_0 l)\exp(-\omega^2)]\exp(-\omega^2)d\omega}{\int \exp[-\omega^2/\alpha^2 - (k_0 l)\exp(-\omega^2)]d\omega} \qquad (7)$$

where $\alpha = (Te/Ta)^{.5}$

$\omega = 2(\nu - \nu_0)/\Delta\nu_d(\ln 2)^{.5}$

ν = frequency

ν_0 = line center frequency

$\Delta\nu_d$ = doppler half width

Te = effective temperature of emitters

Ta = effective temperature of absorbers

$(k_0 l)$ = optical depth

as developed by W. Pendleton and A. W. Shaw at USU. The denominator represents the intensity profile of the emitted radiation ($\exp(-\omega^2/\alpha^2)$) with the effects of the line center preferential absorption included ($\exp[-(k_0 l)\exp(-\omega^2)]$). The self absorption increases as the signal propagates through the medium (as optical depth increases).

The denominator represents the actual line shape frequency profile after propagating thru the medium to the absorbing atom.

The numerator represents this same term from the denominator multiplied by a pure doppler absorption profile ($\exp(-\omega^2)$). The entire equation then represents the normalized overlap of the doppler absorption profile with the self-reversed transmitted emission profile.

This effective microscopic cross section is calculated for assumed optical depths of 0.0 to 19.5, in increments of 0.5. A plot is then made of cross section versus optical depth, for temperatures of 200 to 1000 K, in 100 K increments (Figure 7, at 300 K).

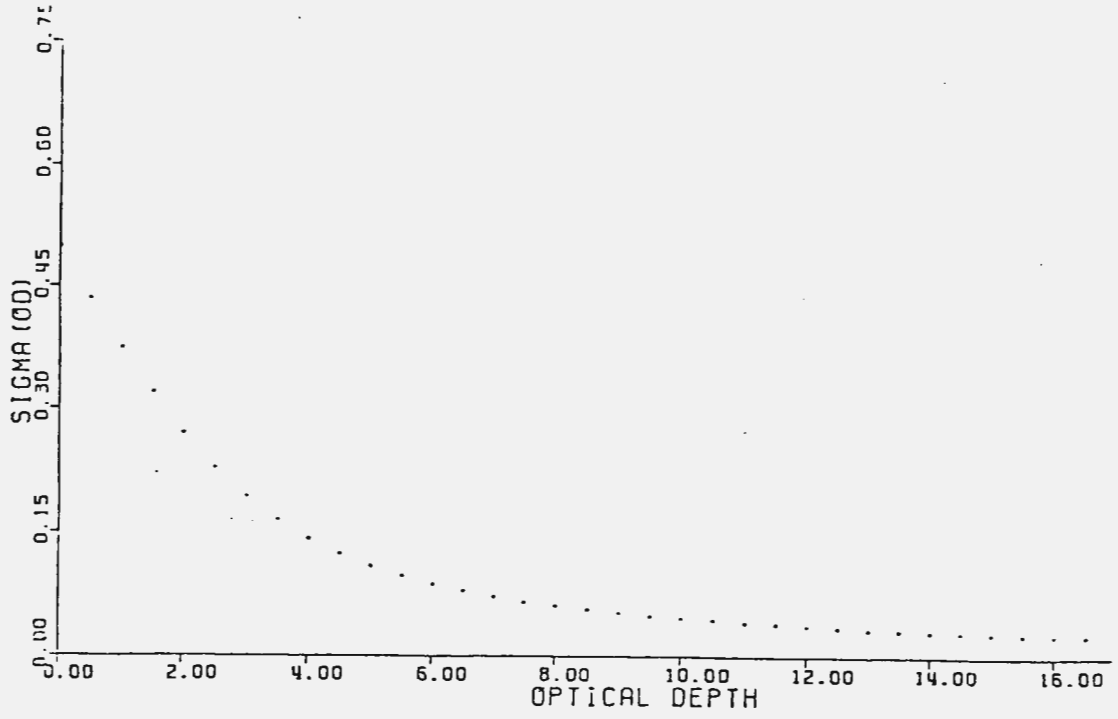

Figure 7. Effective microscopic cross section.

In these programs, a lamp temperature of 900 K is assumed.

Second Order Scattering

A data file containing information about the instrument configuration is neccessary to run the fifth program of the model, GSCAT. GSCAT generates second order scattering information using measurements of the detector radius, detector aperture radius, angle between source and detector, etc. The method used to determine second order scattering considers the solid cone described by the lamp as a source for scattering radiation toward the detector solid cone. Each solid cone is described by the instrument's opening and its baffle aperture. The model considers the source cone to be divided into ten disks, starting at the rocket skin. Each disk is 1 cm thick. The detector cone is divided into 100 disks, starting at the rocket skin, and again 1 cm thick. Each source cone disk is considered a source point of radiation to each detector disk. The program GSCAT computes the physical geometry considerations between each source and detector disk.

Since the detector and source lamp have a finite length and view the atmosphere through a baffle, there will be an unoccluded solid cone surrounded by a solid cone where the signal is partially occluded. The occlusion of the signal is shown in Figure 8.

GSCAT uses only the unoccluded cone to calculate the radius of each disk. The radius is calculated at the center of the 1 cm disk, and the volume of each detector disk is calculated from this radius. The ratio of the area of the detector opening to the area of a sphere with radius equal to the distance between the detector opening and the detector disk is calculated for each disk. This is the solid angle of the detector as viewed from the detector disk and is stored along with the volume of each detector disk. The distance from each detector

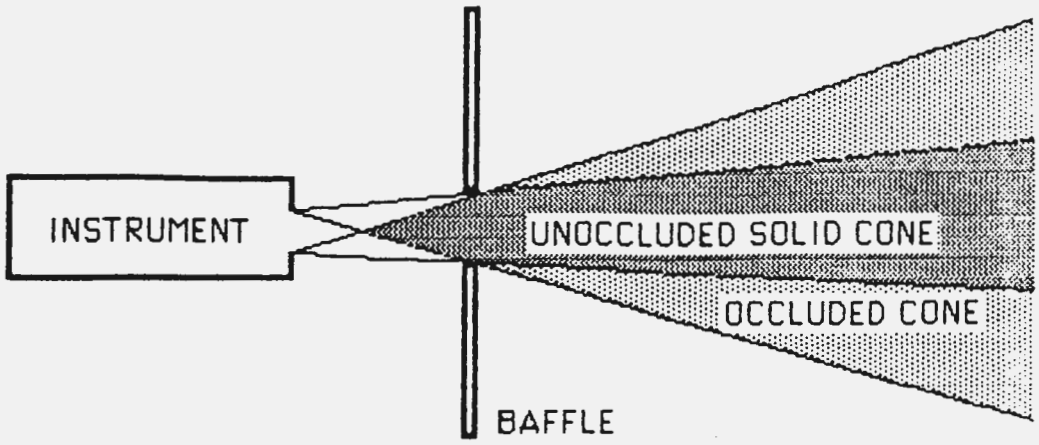

Figure 8. Occlusion of lamp and detector.

disk to each source disk is calculated next. This is done by using the average between the distance from the center of the source disk to the upper inner radius of the detector disk and the lower inner radius of the detector disk. The inner radius is defined as the square root of two times the actual radius. The volume of each detector disk, ratio of areas of each detector disk, and the distance from each source disk to the detector disks are saved in a data file to be used by the next program.

The sixth program, SCAT, uses the information produced in GSCAT to calculate the second order scattering. This is done using measurements of the source radius, source aperture radius, etc. SCAT also uses the data files produced by SIGMA and ATTEN. Each source cone disk radiates to each detector disk, and all detector disks then radiate back to the detector. The radiation is not attenuated from

the source disk to the detector disks, or from the detector disks to the detector. This in an approximate way takes into account multiple scattering using conservation of photons.

The model assumes a lamp source intensity of 1×10^{13} photons per second-steradian on the lamp axis. As previously mentioned the line intensity relative profile of the resonant transitions used is 4.3:2.7:1. The departure of the theoretical 5:3:1 profile is an indication that the doppler frequency profiles of the three lines have suffered self-reversal. The larger the departure from the theoretical ratio, the more self-reversal of the frequency profiles. A data file containing increasing oxygen densities and temperatures is read into SCAT. Then a counts per second value is calculated for second order scattering. This is done by first calculating the intensities of each of the three resonance lines using the assumed intensity on the axis of the lamp and the statistical weights. Since 4.3 + 2.7 + 1 equals 8, this simply means that the intensity of line two would be 2.7/8.0 times the lamp source intensity. The other lines would be 1./8.0 and 4.3/8.0 times the lamp intensity.

Since the off-axis intensity of the lamp usually decreases with distance away from the axis, an average intensity reaching the source disk is used. The decrease of intensity with angle from the source cone axis is found using the angle at which the output of the lamp is almost zero. The angle used in the computer program is 0.5585 radians or about 32 degrees. In measuring the off-axis intensity for the lamp flown on one of the rockets to be analyzed (Tracer), an increase of intensity from the axis to about 9 degrees was found. The average intensity over the area of the source disk is found by averaging the

on axis intensity with the intensity at the edge of the radius of the disk. This average value times the solid angle yields the unattenuated photons per second reaching each source disk from the lamp for each of the three resonance lines.

For each oxygen density assumed, calculations are done for temperatures of 200 to 1000 K in 100 K increments. Each temperature has a cross section and attenuation data file associated with it. Uncertainties arise in the calculation of the optical depth of the medium. The form used for optical depth [Strickland and Donahue, 1970] requires knowledge of 1) density of oxygen atoms, 2) line center cross section for oxygen atoms, 3) distance signal must travel through the medium, and 4) population densities of absorbing oxygen atoms in the ground state triplet. The relative population densities of the three states are assumed to be [Strickland and Donahue, 1970]

$$p(j) = \frac{g(j)\exp[-\Delta E(j)/kT]}{\Sigma_i g(i)\exp[-\Delta E(i)/kT]} \tag{8}$$

where $g(j)$ = the statistical weights of 1, 3, 5

$\Delta E(j)$ = energy difference between j and excited state

k = Boltzmann's constant

T = temperature of the absorbing atoms

This yields the three relative population densities for the three ground states of

$$p(1) = \frac{\exp(-326/T)}{5 + 3\exp(-228/T) + \exp(-326/T)} \tag{9}$$

$$p(2) = \frac{3\exp(-228/T)}{5 + 3\exp(-228/T) + \exp(-326/T)} \tag{10}$$

$$p(3) = \frac{5}{5 + 3\exp(-228/T) + \exp(-326/T)} \tag{11}$$

The line center cross section for oxygen atoms is related to the oscillator strength (f value) for cases of equal emission and absorption temperatures by [Strickland and Donahue, 1970]

$$\sigma_0 = \frac{(\pi)\cdot 5 e^2 f}{mc\Delta\nu_d} \tag{12}$$

where m = mass of oxygen atom

f = f value

c = speed of light

$\Delta\nu_d$ = doppler half width

Using a measured f value of 0.046 [Lawrence, 1969]

$$\sigma_0 = 2.1 \times 10^{-13} \ (cm^2) \tag{13}$$

which compares with Strickland and Donahue [1970]. They calculate cross sections between 1.59×10^{-13} and 8.7×10^{-14} cm^2, for temperatures from 300 K and 1000 K respectively.

To account for emission line profiles of different breadth from absorption line profiles, the line center cross section is multiplied by α, the ratio of the emission line breadth to the absorption line breadth. This is approximately equal to the square root of the ratio of the emission atom temperature to the absorbing atom temperature [Mitchell and Zemansky, 1961, pg. 122]. An α equal to one represents equal emission and absorption line shapes. An α greater than unity

represents an emission line with the same shape but broader width than the absorbing line profile. The optical depth is calculated by using the population densities p(j), the oxygen density, and the atomic oxygen cross section.

$$k_0 l = p(i)[O]\sigma_0 l \tag{14}$$

where $k_0 l$ = optical depth

$\sigma_0 = 2.1 \times 10^{-13}(Te/Ta)^{.5}$

Te/Ta = ratio of emission to absorption temperature

p(i) = the population density of state (i)

[O] = oxygen density

l = distance in centimeters from the rocket skin

The optical depth at each source disk is used to determine the attenuation at the disk. Since the attenuation data file has points calculated with optical depths from 0.0 to 19.5 in increments of 0.5, a linear interpolation using optical depth is performed to determine the actual attenuation for the calculated optical depth. This attenuation is then used to determine the flux in photons per second at each source disk. Optical depth at each disk is now used to determine the effective microscopic cross section. Linear interpolation is again used. The cross section is used along with the ratio of the absorber area (detector disk) to that of a sphere of radius equal to the distance between the source disk and the detector disk (solid angle of detector as viewed by the source disk) to determine the flux to the detector disk. The flux to the detector disk times the solid angle of the detector as viewed from the detector disk determines the

flux to the detector. This is shown in equation form as

$$I = \frac{I_0 W(i)[O] V \sigma \sigma_0 R}{4\pi D} \qquad (15)$$

where I = photons per second

$I_0 = (T_0 - T)1 \times 10^{13}$

T_0 = normalized transmission to previous disk

T = normalized transmission to present disk

$W(i) = g(i)/\Sigma_i g(i)$

V = volume of detector disk

σ = normalized effective cross section

$\sigma_0 = 2.13 \times 10^{-13}$

R = solid angle of detector as viewed from detector disk

D = distance from source disk to detector disk

As mentioned previously, there is no attenuation of the signal from the source disk to the detector disk, and from the detector disk to the detector. Thus the second order scattering has been calculated with higher order effects included. A plot of this is shown in Figure 9.

First Order Scattering

The seventh program of the model, ATOX, calculates the first order scattering. ATOX uses the data files produced by SIGMA, and ATTEN, plus the data file containing information about the source and detector geometries. First order scattering assumes that the emitted radiation from the lamp propagates into the mutual volume of the

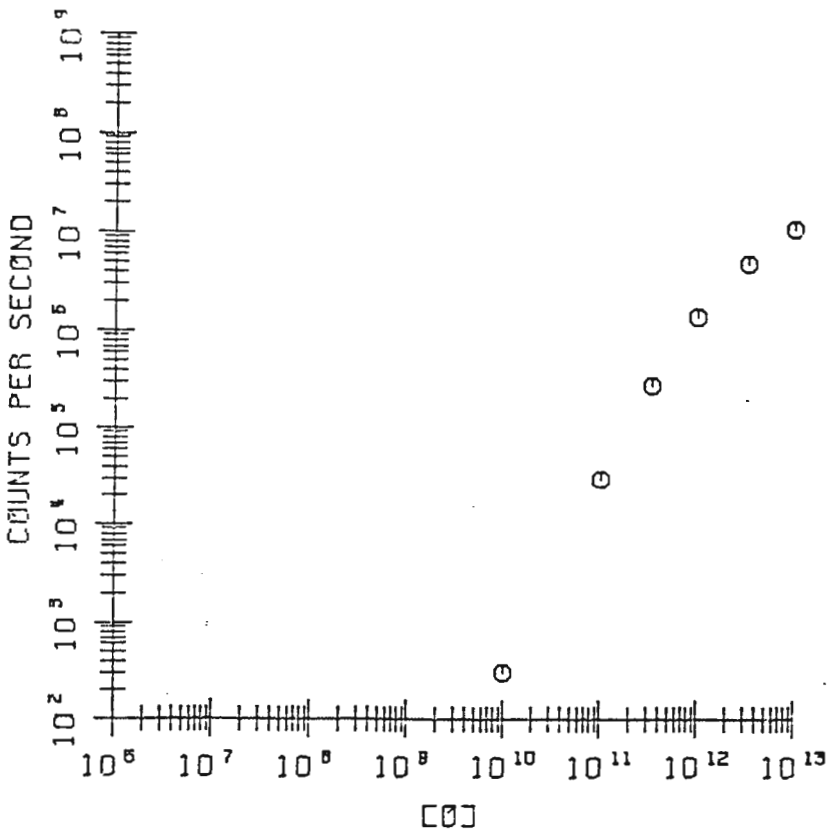

Figure 9. Second order scattering results.

detector and source cones, where a portion of the signal is resonantly scattered once and returned to the detector. The calculation of the returned signal is performed for a differential element inside the volume of intersection between the solid cones of the source and the detector. Integrating over the entire volume of intersection provides the first order scattering results calculated for a given instrument geometry configuration.

First the convolution of off-axis viewing through each instrument baffle is calculated for all angles for both detector and lamp source. The convolution is illustrated in Figure 8, and in Figure 10.

The convolution is dependent only on instrument configuration. Arrays hold all convolution values for later use. As in the program SCAT, control data consisting of oxygen densities and temperatures are assumed. The atomic oxygen cross section is calculated from the temperature using an assumed lamp temperature of 900 K, as was done in SCAT. The population densities are also calculated as they were done in SCAT, using the current oxygen temperature of the control data.

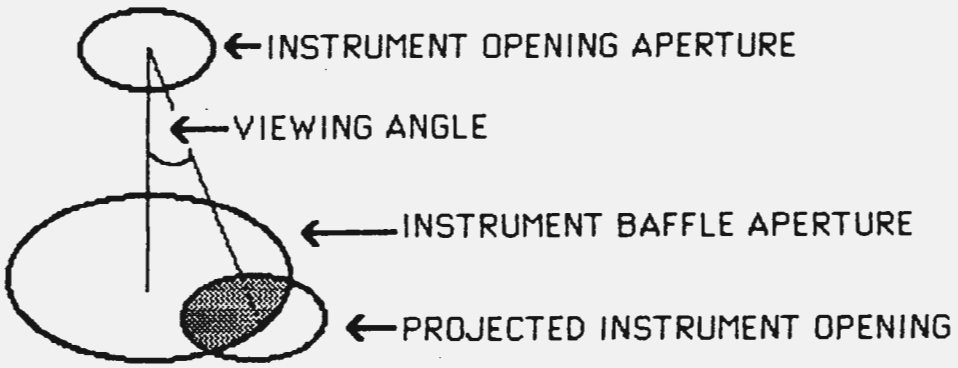

Figure 10. Convolution of a signal seen through two apertures.

The calculations are then split up into the three resonance lines and done for each one. Integration is then performed to step through each differential element. At each differential element the following calculations are performed. Convolution of the signal is determined based on the viewing angle to the source and to the detector. Optical depth is determined based on the distance the signal travels through the absorbing medium. The optical depth is used to calculate both attenuation and the effective microscopic cross section (normalized

overlap function). The above and additional geometry considerations, such as ratio of areas, are used to determine the signal returned to the detector at this differential element. This is shown as

$$I = I_0 W(i)[O]p(i)V\sigma\sigma_0 O_s O_d TS(D/A) \qquad (16)$$

where $I_0 = 1 \times 10^{13}/r^2$

r = distance from source to differential element

V = volume of differential element

$\sigma_0 = 2.13 \times 10^{-13}$

O_s = source occlusion

O_d = detector occlusion

T = normalized transmission

S = off-axis dimming of source

(D/A) = solid angle of detector as viewed from element

D = detector area

A = area of a sphere of radius R

R = distance from detector to differential element

This of course is a theoretical returned signal for an assumed oxygen density and temperature in the absence of a background noise. The integration sums the contribution of each differential element. This is repeated at each oxygen density for the range of temperatures in the model, 200 K to 1000 K in 100 K increments. The oxygen densities begin at 1×10^7 and end at 1×10^{13} atoms per cubic cm. Thus the theoretical return of light emitted by the source lamp from one resonant scattering process is predicted, with functional parameters var-

ying throughout the range of expected values encountered in the altitude region of a rocket flight. First order scattering contribution to the transfer function is shown in Figure 11.

The eighth program, PLOTT, combines the first and second order scattering results to create the final transfer function. For a given oxygen density, the instrument response in counts-per-second is plotted. As mentioned above, the oxygen density input ranges from 1×10^7 to 1×10^{13} atoms per cubic cm. This plot is made for temperatures ranging from 200 K to 1000 K, in 100 K increments (Figure 12).

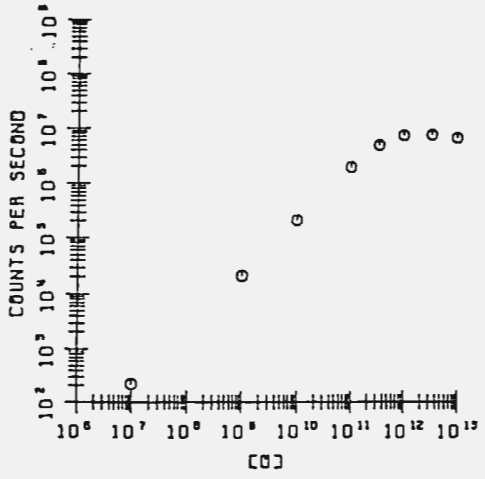

Figure 11. First order scattering results.

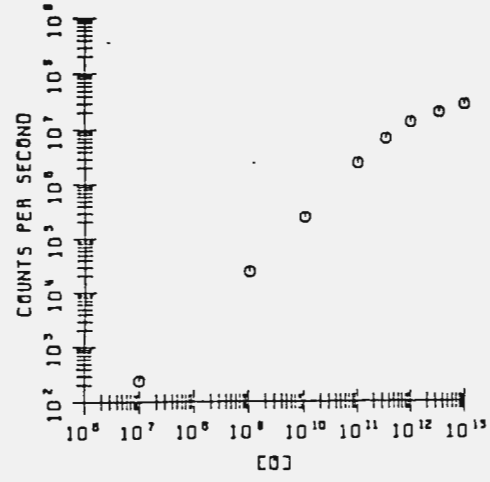

Figure 12. Transfer function.

CHAPTER IV

TRANSFER FUNCTION INTERFACE WITH DATA

The interfacing between the transfer function and rocket flight data is done in one program with a generic name of FINAL. This program uses a measured or best known temperature profile to determine the temperature of the atomic oxygen scattering the radiation. FINAL also uses the measured voltage of the lamp intensity monitor to take into account lamp intensity variations during flight. Linear interpolation is performed on temperature using the measured temperature to interpolate between the model results which are presented in 100 Kelvin increments. FINAL has the option of reducing the data with various averaging parameters. Reduction can be done using time or altitude as the incrementing parameter. Two parameters are used for either increment type. 'Every' is the parameter which determines how often a point is plotted. 'Over' is the parameter which determines how many points to consider when averaging. For example, choosing altitude as the incrementing parameter, 'every' equal to 1, 'over' equal to 2, reduces the data by averaging data points over a 2 km altitude change, and performing this operation every 1 km. Time increments are in units of seconds.

There is a FINAL program for each of the three rocket flights. FINALEC (for final Eclipse) reduces data for the 1979 Eclipse flight from Red Lake, Canada. FINALAN (for final Andoya) is for the Andoya, Norway flight. FINALTR (for final Tracer) reduces the data from the Wallops Island, Virginia flight nicknamed 'Tracer'. The differences between the programs include flight data for both a temperature pro-

file over altitude, and a lamp intensity profile over time. Another difference included is calibration factors for the specific instrument geometry flown.

Calibration

First the raw counts are averaged over the desired distance. A conversion factor accounting for the time frame of measurement and calibration of the instrument changes the raw counts average into a counts per second average. The calibration procedure involves placing the detector a measured distance from the lamp source. Then the assumed count rate from the computer program is multiplied by the solid angle of the detector as viewed from the lamp. This predicts the theoretical count rate of the measurement with the lamp emission rate assumed in the computer program. Then the lamp is turned on and the detector response is recorded. The ratio of the theoretical response to the measured response provides the calibration of the lamp-detector system. If the flight measurements are made over 0.016 second intervals, to convert the detector response into counts per second the response is divided by 0.016.

Temperature

The altitude associated with a data piece is used to linearly interpolate a temperature from the measured flight temperature. The flight temperature is usually stored in 1 km increments, so the interpolation is done between 1 km temperature differences. This is usually a small quantity (between 1 and 15 Kelvin).

Lamp Intensity

Next, a linear interpolation is performed on the lamp intensity monitor. Data for the flight lamp intensity profile is stored using time increments. The lamp intensity usually changes very slowly. This allows a very large time increment to be used when storing the lamp intensity profile, and 35 seconds is usually used. A plot of the Andoya, Norway flight lamp intensity monitor is shown in Figure 13.

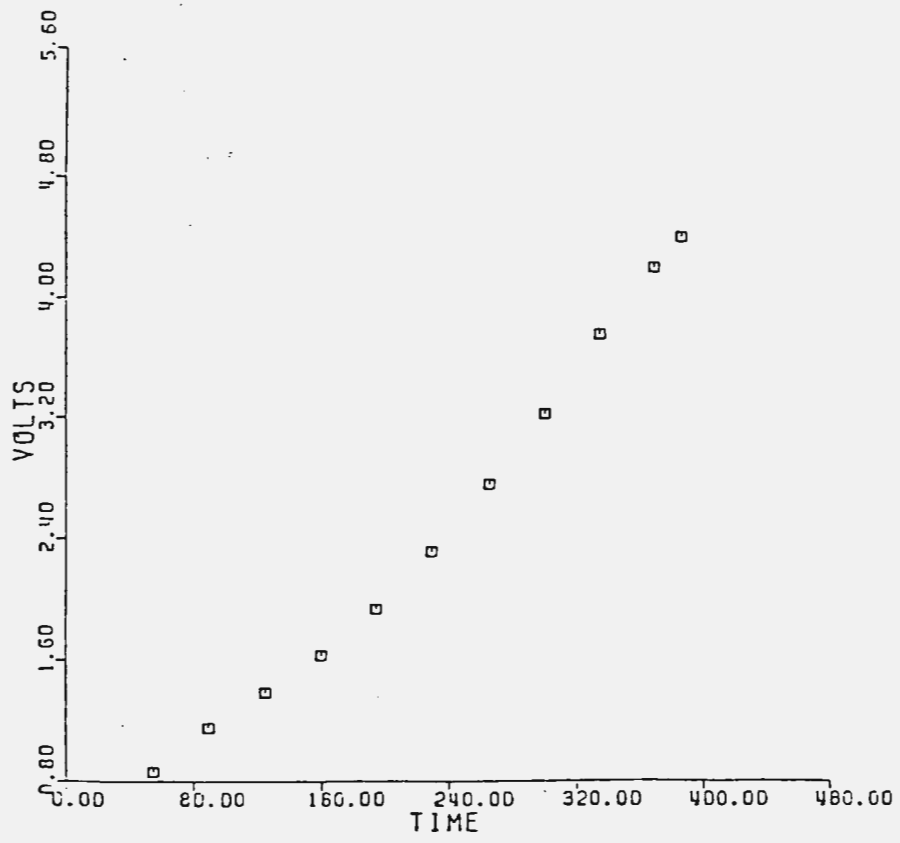

Figure 13. Lamp intensity monitor.

The time associated with the current data average is used to interpolate to find the operating voltage of the lamp for this data piece. This is then used to account for differences in the lamp voltage from when calibration occured.

Interpolation of the Transfer Function

Finally the transfer function is used to determine an oxygen density from the counts per second average. The transfer function calculates eight atomic oxygen densities from eight counts per second values. The FINAL programs interpolate between two successive counts per second values using the calculated average from the rocket flight data. Since the transfer function is calculated at 100 Kelvin increments, the flight temperature for the particular data piece is used to determine which two temperature transfer functions to read into the program. These two transfer functions are then used to linearly interpolate using flight temperature to determine the actual atomic oxygen density for this particular data average. For example, if the data piece under consideration has a temperature of 350 Kelvin associated with it, the model uses the transfer functions calculated with temperatures of 300 Kelvin and 400 Kelvin. This process is then repeated to cover the altitude range of the flight.

CHAPTER V

ANAYLSIS OF FLIGHT DATA

Eclipse Flight

The first of the three rocket flights under consideration is the February 26, 1979 launch during a solar eclipse. The rocket was launched at about 10:28 CST (16:28 UT) when approximately 40% of the solar disk was visible. Since this was a daytime flight, some solar radiation contamination of the signal can be expected. Since we are measuring a signal in the presence of a background noise, a measurement is taken with the lamp on, and then another measurement is taken with the lamp off. The off value is subtracted from the on value to provide a difference value representing the signal with the background removed. For every two measurements (on and off values) one data point (difference value) is used. Occasionally a data point is measured that is so different from the ones surrounding it that it can only be described as an anomaly in the measurement system. Since it provides no meaningful information and could adversely affect the result of an average, this type of point is labeled a 'bad' data point and thrown away. When discarding data points, they are always thrown out in on-off pairs.

The Eclipse flight had many data points which were much larger than the surrounding points, and were considered to be contaminated. The contaminated data points occured at a rate that closely followed the rocket spin rate which was about 8 Hertz. This led to the conclusion that the signal was contaminated from a point source within the field of view of the rocket in the atmosphere. This contamination was

then attributed to the solar disk. If the percieved solar contamination were constant in intensity, it could easily be removed. However, since the measurement time of the data was 16 milliseconds, and the rocket spins at about 8 Hertz, about three data points per spin were spoiled. Of these points, the solar contamination varied greatly between them. The contamination was also an order of magnitude greater than the measurable signal. Hence the solar contaminated points could not be saved and were discarded. Figure 14 shows the on counts, off counts, and difference counts without the sun looking data.

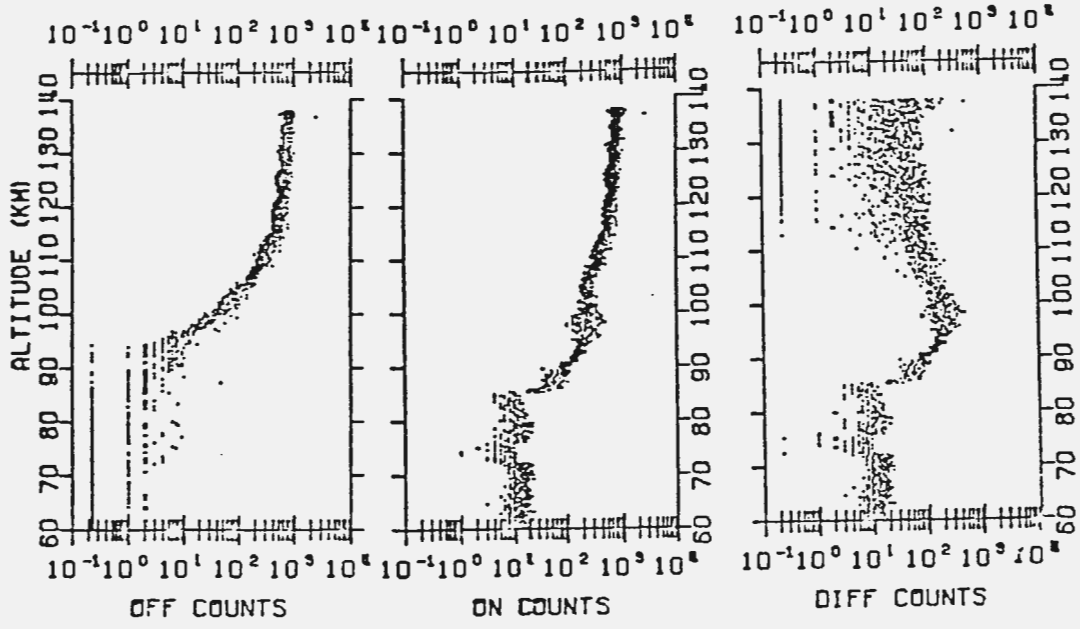

Figure 14. Eclipse raw data.

The off counts plot shows the background 130 nm radiation measured by the detector with the lamp off, which resembles Figure 5 above

110 km. This count rate is a counts per measurement frame (0.016 sec). Any data points equal to zero are plotted to the left of the value 1 on the horizontal logarithmic scale. The on counts plot contains those data points measured by the detector with the lamp on. By comparing the off counts plot to the on counts plot, one can determine where the measureable signal rises above the background. This occurs below about 115 km. When the measureable signal is less than the background noise, the random scatter (spread) of the difference values is large. This is quite apparent in the difference counts plot above 115 km. With such a large spread of points, the accuracy of the measurement is quite questionable at altitudes above 115 km. For the difference counts plot, both zero and negative data points are plotted to the left of 1 on the logarithmic axis. Negative points are obtained when the off value measured is greater than the signal measured with the lamp on.

Another problem resulting from a daytime flight is the resonantly scattered solar 1304 Å radiation. Unlike the solar contamination described above, the resonantly scattered radiation is not located at a point, but is fairly evenly distributed throughout the sky. This is due to the large optical depth that solar 130 nm radiation must encounter to reach altitudes of less than 140 km in the atmosphere. The solar resonantly scattered radiation tends to increase the random scatter in subtracting off counts from on counts. This radiation decreases greatly as altitude decreases, due primarily to absorption by molecular oxygen. Below about 100 km the solar resonantly scattered radiation has little effect. Along with the resonantly scattered solar radiation is Rayleigh scattered solar radiation of fre-

quencies transmissible through the detector filters. This is a small amount and is ignored.

Very much like the resonantly scattered radiation is the aurorally excited 130 nm radiation. There has been a fair amount of documentation of the 1304 Å airglow [Strickland and Donahue, 1970; Meier and Lee, 1982; Anderson et al., 1980]. The results show substantial background 1304 emissions starting at 100 km and increasing with altitude (Figure 5). Specifically the auroral 1304 emissions has also been measured and compared with model predictions [Donahue and Strickland, 1970]. The 1304 Å emission is the brightest single auroral feature in the ultraviolet range [Strickland and Rees, 1974]. Significant energy deposition from particle precipitation at all altitudes above 80 km [Baker et al., 1980] occured during the eclipse. The effects of the aurorally excited radiation are basically the same as the resonantly scattered radiation, increasing the random scatter in the difference between on and off counts. Hence all of the data has somewhat more random scatter than would otherwise be expected.

The instrument configuration for the Eclipse flight was designed at an early stage of development of the oxygen resonant lamp system. Since the transfer function depends greatly on the instrument configuration and little experience from previous flights being available at the time, a nonlinear transfer function resulted. The transfer function becomes nonlinear at higher count rates, but is linear for small count rates. Figure 15 shows the transfer function for the instrument flown on the Eclipse flight. The nonlinearity is seen as a flattening of the transfer function at densities above 10^{12}. This combined with the large daytime background noise created problems in converting

large count rates into oxygen densities. This problem was limited to the region of the largest oxygen densities. At count rates of around

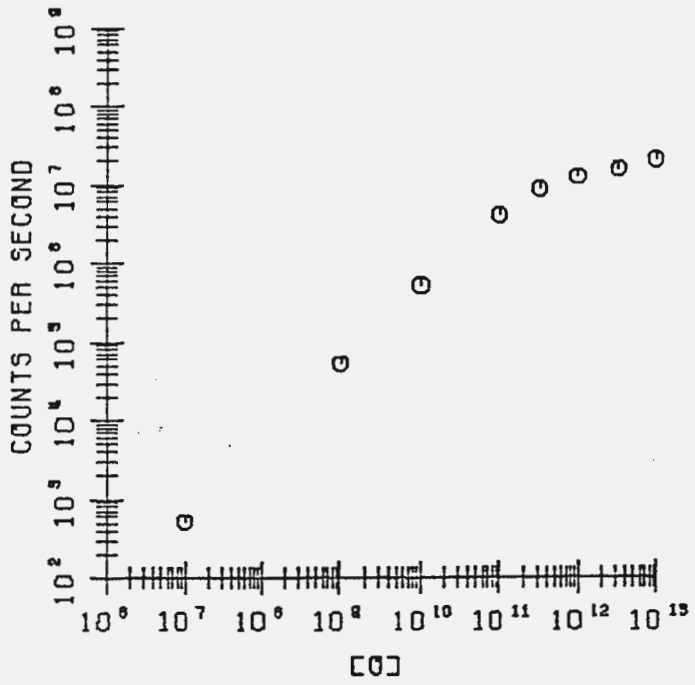

Figure 15. Eclipse transfer function.

10^7 a small error in counts produces a large error in oxygen density.

To compensate for the nonlinear transfer function a weighted mean was developed to minimize errors at large count rates. The ratio of the nonlinear slope to the linear slope of the transfer function was used to define the weighted values assigned to particular count rates. This tends to keep the error bars of the nonlinear region equal to the error bars of the linear region. The transfer function is calculated using eight points, and slopes are defined by straight lines connecting these points. The linear region uses weighted coefficients equal to one. The weighted coefficients decrease to about 0.2 as the nonli-

nearity increases. Hence the extremely large count rates are considered to be less important compared to smaller rates measured in the same region. It is important to note that the weighting of values has no effect at all if all count rates in a particular average calculation have the same weighted coefficient. It is only a weighted calculation if differently weighted count rates occur when calculating an average.

The use of a weighted mean brought out the structure of a double peak which was previously unseen. The peaks are at 94 km and 100 km, and previously were seen as one peak at 96 km. Figure 16 shows the original reduction (figure on right) compared to reduction using the weighted mean (figure on left). The double peak structure is quite obvious when using the weighted mean. This seems resonable since many measurements of atomic oxygen have shown double peaks or similar structure at approximately these altitudes [Philbrick, et al., 1973; Philbrick et al., 1974]. A measured structure such as the mass spectrometers used by Philbrick is more easily believed than an inferred structure derived from assumed quenching and production rates as is necessary in the 5577 Å photometers. Dickinson et al. [1980] has also measured quite a variety of structure using the resonant lamp technique, so it seems that fine structure on the order of 5 km or so can be a common feature of atomic oxygen density profiles at the altitude region of the peak density. The use of the weighted mean also decreases the peak density slightly. The Eclipse flight also shows a slight bulge at about 120 km as has been seen in measurements [Philbrick et al., 1974] and models [Dickinson et al., 1976].

A common characteristic of atomic oxygen density profiles is the sharp drop in density at approximately 85 km as is easily seen in the Eclipse flight (Figure 16). There is also an interesting shoulder or

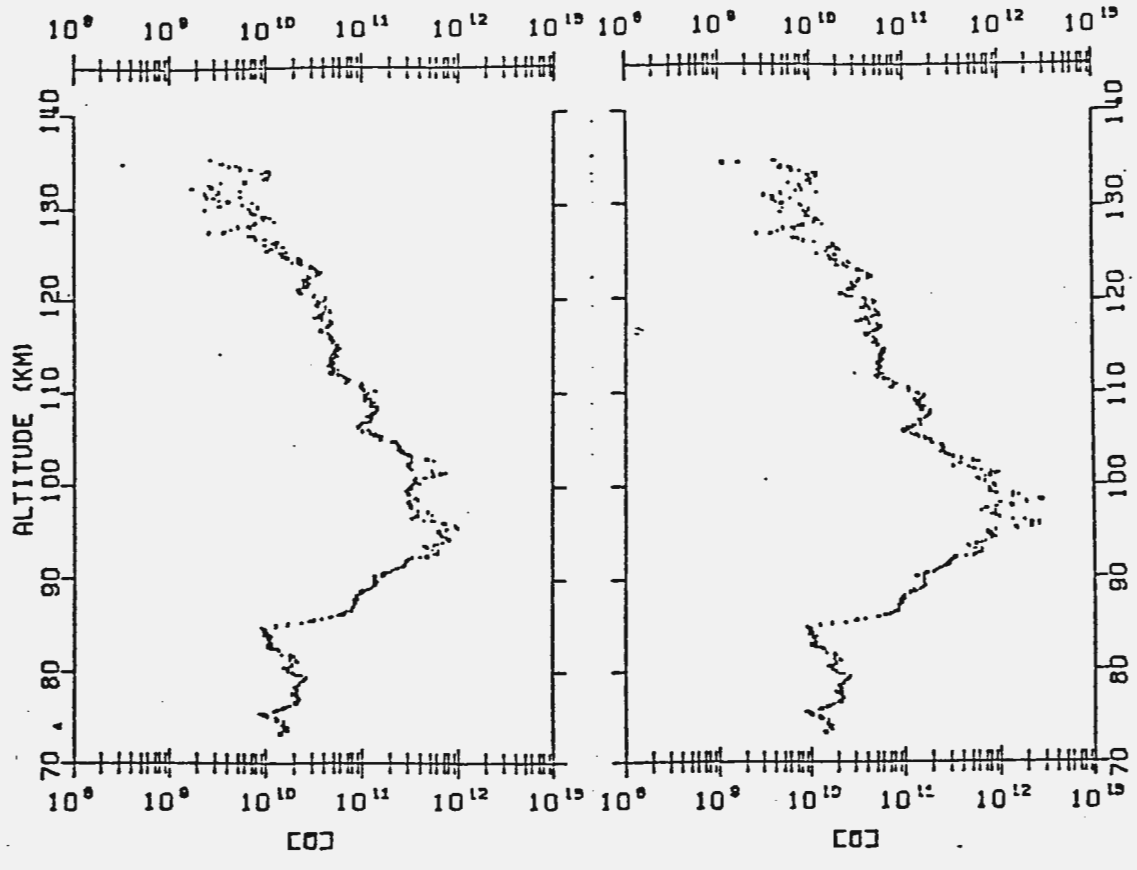

Figure 16. Eclipse flight weighted mean comparison. The data was reduced using a running average over distance, plotting a point every 0.15 km, and averaging over 1 km.

step in the density profile from 87 to 89 km. Stepwise increases in density have been previously reported by Dickinson et al., [1976]. Below 85 km the density remains fairly constant between 1 and 2 x 10^{10}, as is typical of daytime profiles.

Andoya Flight

The second flight under consideration is the Andoya, Norway flight. The rocket was launched 4:15:59 GMT on November 16, 1980, as part of the Energy Budget Campaign. Since this winter flight was launched at a region of high latitiude, a night profile for atomic oxygen was expected. The Andoya flight did not have the problem of direct solar contamination that caused many data pairs to be rejected in the Eclipse flight. There is small background noise caused by Rayleigh scattering and auroral contamination similar to the Eclipse flight. Again this auroral contamination was restricted to altitudes above 100 km.

When subtracting off counts from on counts there occured an abnormally large number of negative difference values. This was attributed to a non-50/50 duty cycle on the lamp on/off sequencing. This problem was dealt with by artificially changing the duty cycle such as to produce an average of zero at the peak altitude that the rocket attained. The reasoning behind this was that there should be so little atomic oxygen at 180 km that in effect our measurement system should measure a zero density there. The method used to change the duty cycle was to multiply the measured on count value by a number larger than one, 1.002 for example. This number represents an on duty cycle of 0.501. For conservation reasons the off counts would then be multiplied by 0.998, which represents an off duty cycle of 0.499. This is so that the actual count rate is not artificially increased. In other words, we have to take time away from the off count cycle to give it to the on count cycle. Now that an on/off duty cycle of 0.501/0.499 has been used, the off counts are subtracted from the on

counts to provide the difference count value. This would mean that the actual on/off duty cycle that the lamp operated at was close to 0.499/0.501. This was a simplistic example, and the on duty value used to reduce the Andoya flight data was equal to 0.501365.

Another problem encountered in the Andoya flight was an modulation in the data at about the rocket spin rate of approximately 8 Hertz. As was mentioned earlier, a modulation in the data at the spin rate of the rocket indicates that more 130 nm radiation reaches the detector from one direction relative to other directions. Since this flight occured at night, the fluctuations could not be attributed to the solar disk, as they were for the Eclipse flight. The Andoya flight was launched after a time of intense auroral activity. It is difficult to believe that auroral 130 nm radiation was not isotropic after the intense activity, since the optical depth is large. If the 130 nm radiation was not isotropic, the random scatter of the measured signal would increase in one direction, yielding an oscillation at the spin rate. An interesting point is that the oscillation occurs over the entire flight, including when the door of the rocket was still closed. With the door closed the instrument does not have access to outside the rocket skin. This seems to be a contradiction since the only imaginable source for oscillation in the signal should be outside the rocket.

The instrument geometry for Andoya was designed so that the volume of intersection between the lamp axis and the detector axis began at the rocket skin. Unfortunately this allowed measurement of oxygen atoms disturbed by flow effects near the rocket skin. Since the rocket travelled at supersonic speeds the disturbed oxygen atoms

have different characteristics than the undisturbed ambient oxygen. Outgassing from the rocket skin and high velocity collisions of the rocket with atmospheric molecules contribute to the wake effect near the rocket skin. However, since the oscillation of the Andoya data occured even with the rocket door on, the cause of the oscillation is not clear. This anomaly was essentially ignored. The oscillation increased the scatter when the returned signal was less than the background, but had little effect on the profile when the returned signal was much greater than the background (85 to 100 km) as is seen in Figure 17.

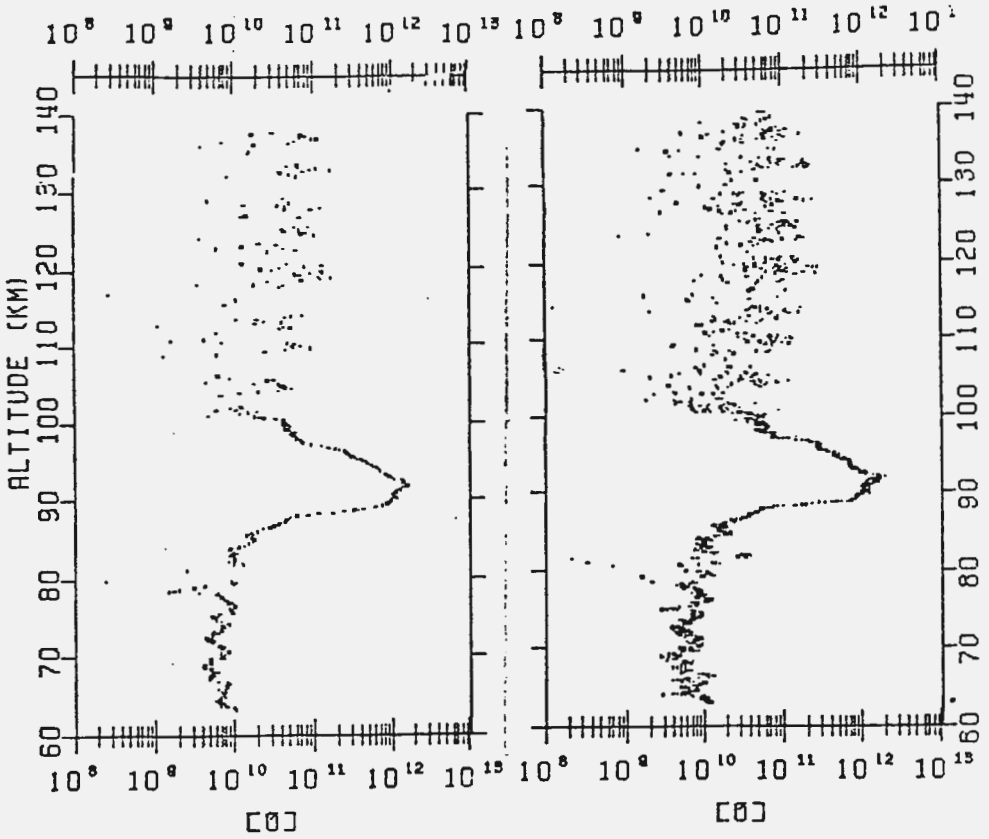

Figure 17. Andoya flight density profile. A running average was used in reducing the data, plotting a point every 0.15 km and averaging over 1 km for the figure on the left, and plotting every 0.05 km and averaging over 0.5 km for the figure on the right.

Since a believable reason for the oscillation was not discovered, we did not feel justified in removing it.

A rather large low altitude signal occured in the Andoya data which appeared as if we were measuring a dawn density profile. Dickinson et al., [1976] has clearly shown that a dawn profile has a minimum density at 79 to 80 km with appreciable buildup below 79 km. This is exactly what the Andoya flight profile exhibits. A typical night time measurement decreases at altitudes below 80 km at a fairly sharp rate. This is because there is little production of atomic oxygen at low altitudes at night. The density falls to below the measurement capability of the system very quickly yielding virtually no signal. However during daylight hours there is a fairly large constant production rate of atomic oxygen. The daytime profile of atomic oxygen has fairly constant densities below 75 km. The dawn-like profile of Andoya exhibits another anomaly for this flight, although others [Perov and Rakhmanov, 1977] have measured large night time low altitude densities.

Comparing the raw on and off data counts provides useful information on when the measured signal rises above the background noise level. It is fairly obvious from Figure 18 that there is definitely a signal being measured below 80 km. It is also obvious that the noise level increases above the signal level at about 100 km. Information is not very meaningful in converting the counts to oxygen densities above that altitude. Any result obtained is going to be largely influenced by a random scattering of points as is easily seen from the difference counts plot of Figure 18.

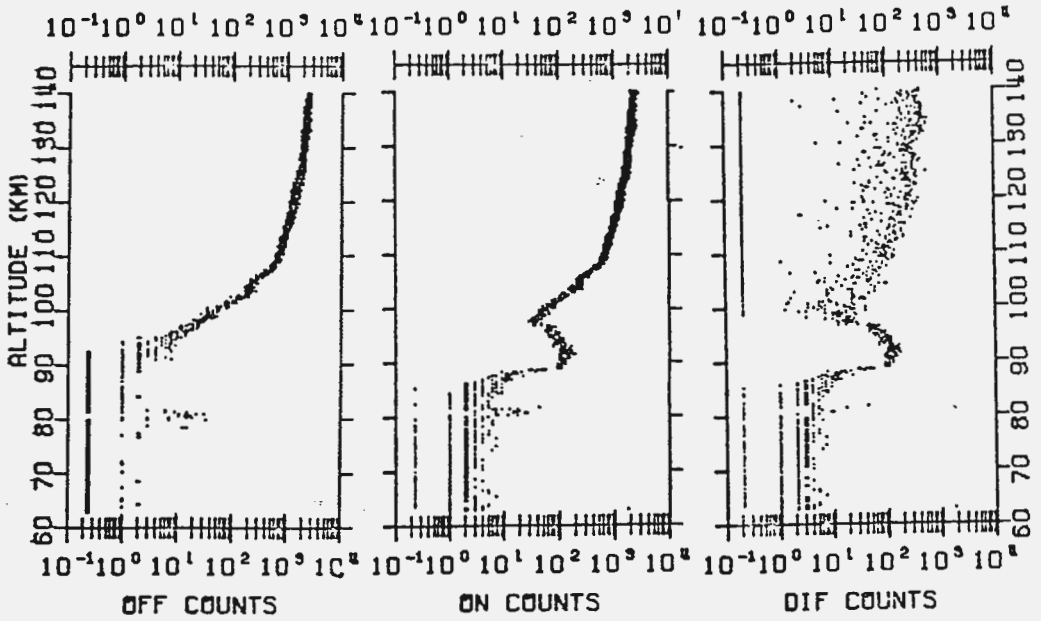

Figure 18. Andoya raw data.

Also seen in the plots of raw counts is an interesting spike at 80 km. This is another unexplained result in the Andoya data. However this spike occurs at an altitude of less interest than the peak altitude.

Tracer Flight

The last flight under consideration is the Wallops island, Virginia flight named Tracer. This flight was launched 11:00:59 EST June 29, 1982. Since this was a daytime flight the characteristic low altitude profile of a constant density should be expected. The rocket door opened at 68 km, but above that a definite signal occured remaining fairly constant up to 85 km. There is definitely a modulation on the signal, but this time it occurs with approximately a 13 second

time period and is visible over the whole flight. A plot of the raw difference counts over time is shown in Figure 19.

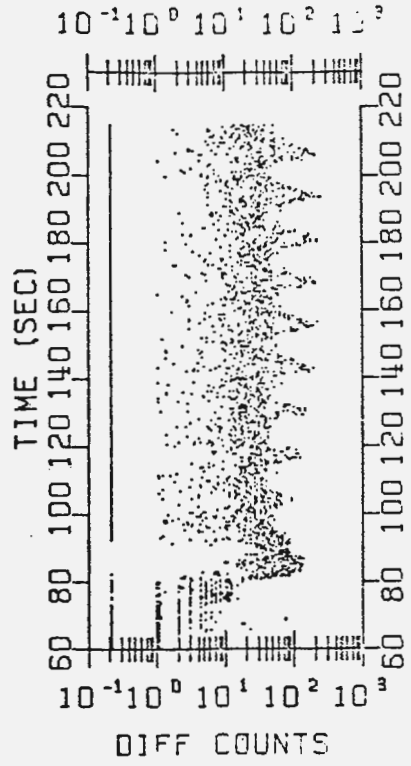

Figure 19. Tracer raw data.

Plotting the data over time instead of altitude emphasizes the constant period of oscillation. The oscillation was obviously not at the spin rate, but it does correspond to the precession rate of the rocket. Since this was a daytime flight, it seems reasonable to conclude that the rocket instrumentation viewed a portion of the solar disk during the precession. It is easy to see that the effect of the contamination was large at altitudes above 110 km. The amplitude of the effect decreased with decreasing altitude. Figure 20 shows the raw data for the Tracer flight plotted over altitude, with the contaminated points included. As the altitude increases to about 90 km, the

signal rises above the contamination. Hence the contamination has little effect on the measurement of the peak density.

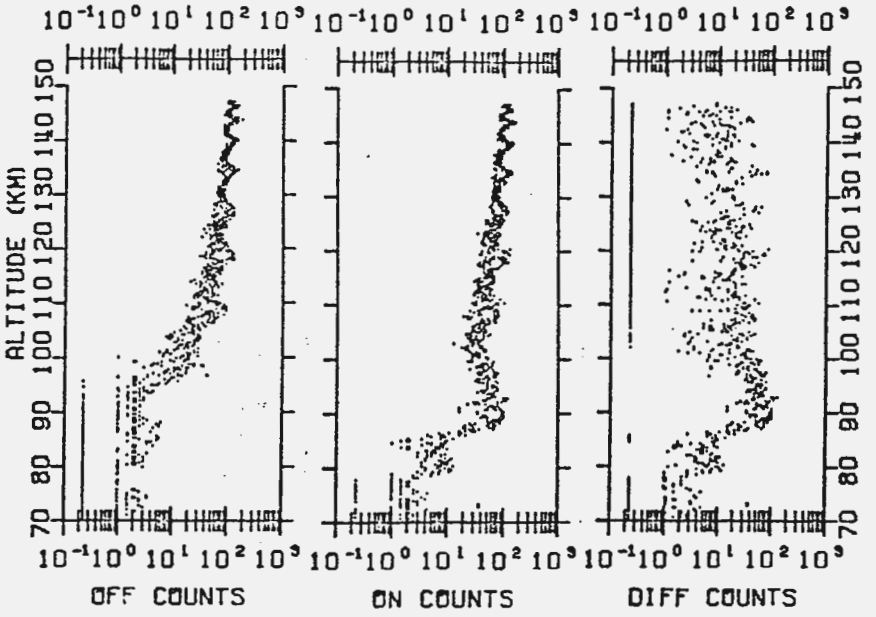

Figure 20. Tracer raw data over altitude.

Altitudes above 110 km again are less reliable as the background noise level was higher than the measurable signal resulting in an abnormally large number of negative averages in the high altitude region. A duty cycle was used to compensate for this effect as used for the Andoya flight. The Tracer duty cycle used had an on/off ratio of 0.51285/0.48715.

There seems to be a spike in the low density direction at 74 km as seen in Figure 21. The spike does not seem to be correlated with the solar contamination. There is also a very interesting structure in the 90 to 105 km region. The structure can not be correlated to

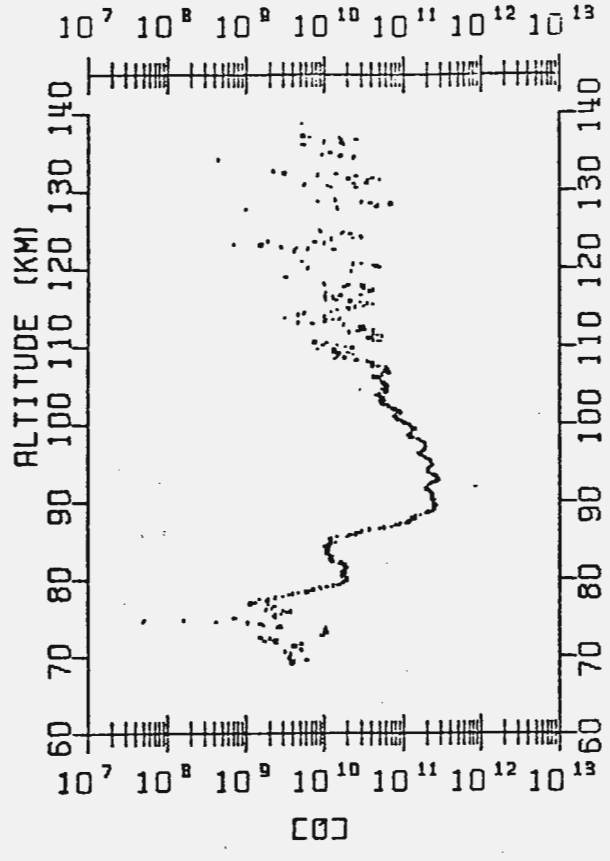

Figure 21. Tracer flight oxygen density profile. A running average was used in reducing the data, plotting a point every 0.15 km and averaging each point over 1 km.

either the rocket spin or precession.

There has been some discussion on the wave-like structure measured in electron and neutral density profiles [Dyson, et al., 1970; Newton, et al., 1969]. Severe weather conditions can cause acoustic waves [Georges, 1968], and Georges has suggested that incoherent superposed gravity waves propagate to ionospheric altitudes from below.

Gravity waves, turbulence or wind shear may be invoked to cause the wave-like structure [Dickinson et al., 1980]. The altitude range between 90 and 130 km has been described as a highly dynamic region, with half wavelengths of about 6 km below 105 km [Trinks et al., 1978]. Dickinson [1980] reported wavelengths between 1 and 10 km. The Tracer data shows wave-like structure between 90 and 105 km with a wavelength of about 2 to 3 km. Above 110 km the scattering of the signal increases due to solar resonantly scattered and dayglow background noise. Another interesting feature is the shoulder at 80 km. This shoulder takes on various shapes in different flights, the Eclipse flight for example, but has definitely been seen a few times. In the Tracer flight the shoulder includes a minimum at 85 km, which is a quite common feature in atomic oxygen profiles.

The Tracer flight used rectangular baffles to increase the volume of intersection between the source cone of view and the detector cone of view. The convolution of a signal through a circular aperture and a rectangular aperture is shown in Figure 22. The rectangles were short in the vertical direction and long in the horizontal direction. This increases the volume of intersection and hence sensitivity of the instrument without bringing the volume closer to the rocket skin. Flow effects close to the rocket skin can produce undesirable results in the data. Enlarging the volume of intersection far from the rocket also is not desirable since the emitted radiation decreases in intensity as it penetrates farther into the medium. The farther the signal travels through the atmosphere, the larger the optical depth. Since our assumptions in deriving the transfer function become questionable at large optical depths, this is not a desirable option. Using

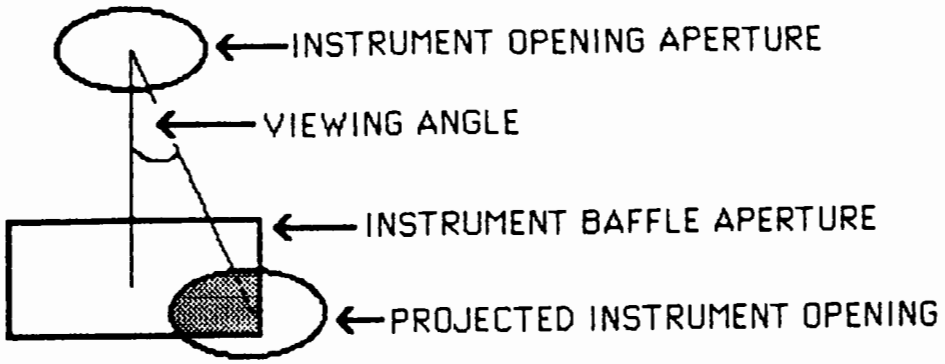

Figure 22. Convolution of a signal seen through two apertures (one rectangular).

rectangular baffles resulted in the best transfer function to date in the model (Figure 23).

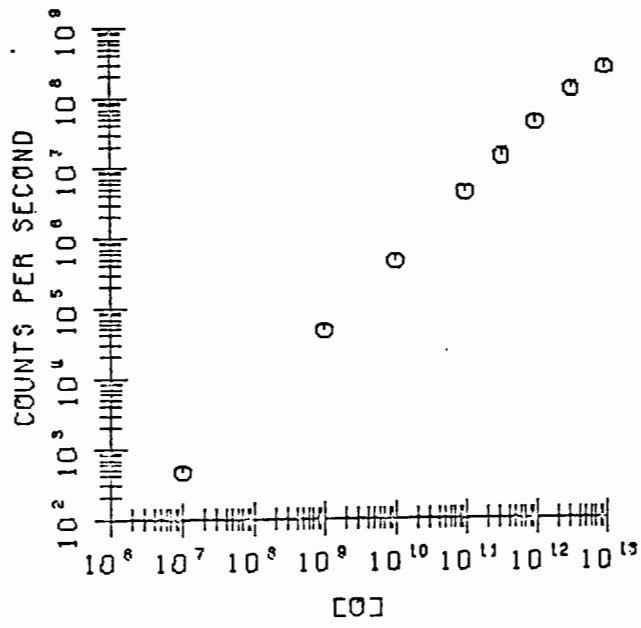

Figure 23. Tracer transfer function.

The transfer function remained fairly linear to count rates of 10^8. Because of this there was no problem in measuring the peak density for the Tracer flight.

Comparison

Figure 24 shows all three flights on the same plot for comparison.

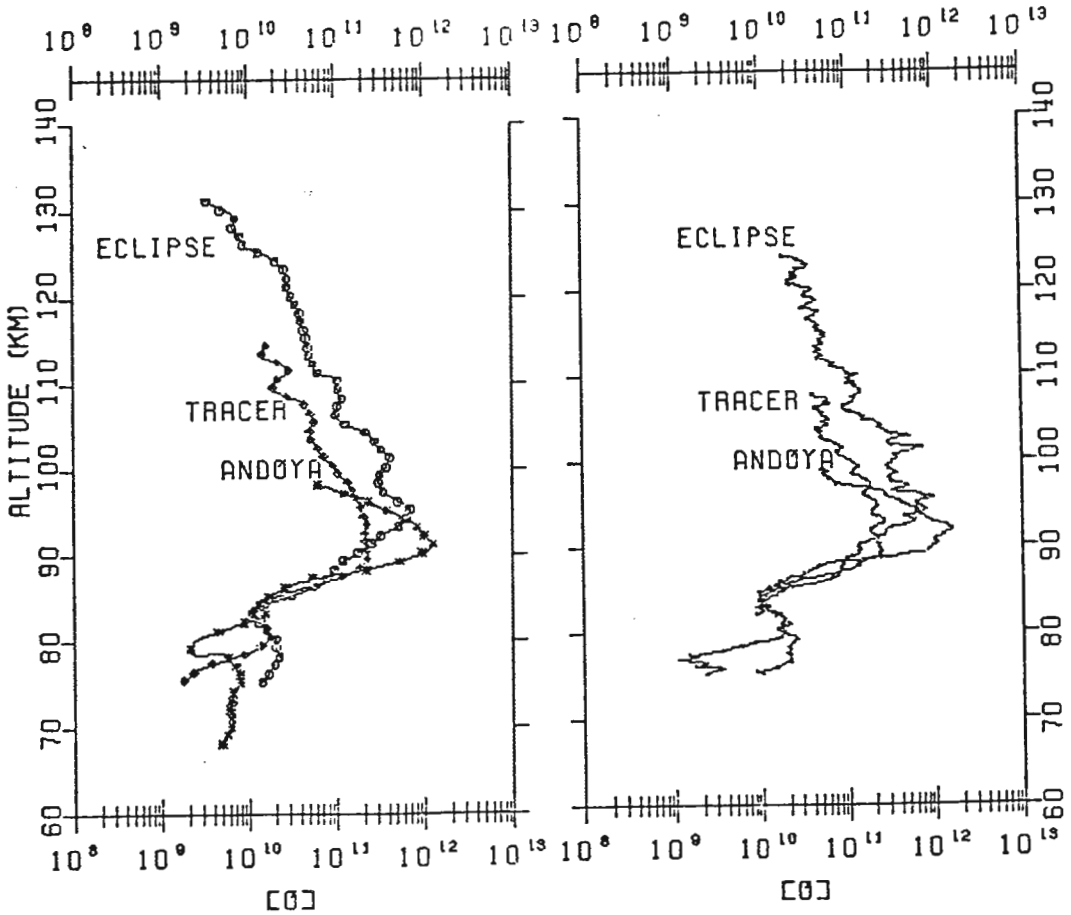

Figure 24. Density profiles of the three flights. A running average was used to reduce the figures. The figure on the left plots a point every 1 km and averages over 3 km, and the figure on the right plots a point every 0.15 km while averaging over 1 km.

The altitude range of each flight was limited so as not to include large random scattering which would complicate the figure. The main

features of the three flights are seen in the figure. The Eclipse flight exhibits the double peak (or large 8 km wavelength fluctuation between 95 and 110 km). The Andoya data show a sharp peaked profile and a fast drop in density above the peak. The Andoya profile also shows a minimum density at 79 km, with a constant density below that. The Tracer data has a flat peak at lower densities than the other two flights. The wave-like structure of the Tracer flight is lost using large averaging distances, but is clearly indicated for smaller averaging distances. Since the structure is maintained even for averaging distances of 0.05 km, the wave-like profile is believed to be real.

In each of the three profiles the oxygen density drops rapidly in the 85 km region as has been measured by Dickinson et al., [1980] and others. This seems to be the most common feature between all atomic oxygen density profiles. In contrast, the peak profile in each flight is distinctively different. The Eclipse flight shows large scale (8 km) variations, the Tracer profile oscillates with about a 2 km wavelength, while there is no oscillation at all on the Andoya peak profile. Figure 25 presents the peak density region (86 to 104 km) for the three flights, along with a demonstration of the effect of different averaging distances. The large scattering inherent in the profiles using small averaging is the major limit to the resolution of the resonant scatter technique. However the use of a range of averaging distances is useful in supporting the validity of structure unaffected by the changing of the averaging distance. The peak density altitude of the three flights ranged from 92 to 95 km, which is in the range usually reported. Dickinson et al., [1980] has measured peaks between 90 and 98 km for twelve flights of the resonant scatter tech-

nique. Repeated satellite measurements of a peak density altitude of 95 plus or minus 4 km have been reported [Donahue and Guenther, 1975].

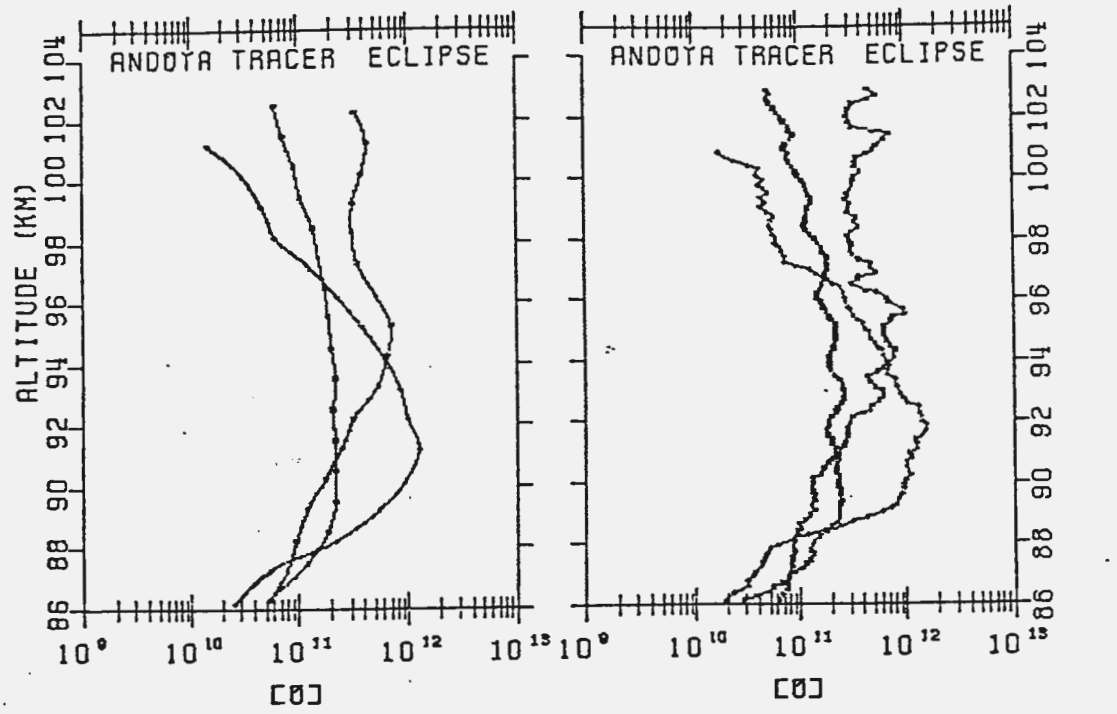

Figure 25. Peak density profiles for the three flights. A running average reduced the data, plotting every 1 km and averaging over 3 km for the figure on the left, plotting every 0.15 km while averaging every 1 km for the figure on the right.

Golomb and Good [1972] have measured peak density altitudes at 95 km plus or minus 2 km using nitric oxide releases. There is some controversy as to whether the peak density altitude is seasonally dependent [Offermann and Drescher, 1973; Donahue and Guenther, 1975; Offermann and Drescher, 1975]. Dickinson et al., [1980] measured no obvious seasonal dependence of the peak density altitude. With only three flights, the USU results are too few to speculate a seasonal change.

Latitude variations of the [O] profile have also been reported [Donahue, et al., 1973; Wasser and Donahue, 1979; Forbes and Marcos, 1980]. The extremely dynamic nature of the oxygen profile near the

peak has been recognized [Trinks et al., 1978], and Philbrick et al., [1973] has suggested that atmospheric dynamics are important in determining [O] profiles. The data obtained by USU demonstrates the wide variety exhibited by atomic oxygen density profiles.

CHAPTER VI

ERROR DISCUSSION

This chapter attempts to describe the errors characteristic to USU's resonant scatter measurement of atomic oxygen in the upper atmosphere. The type of errors encountered may be divided into two groups, random and systematic. The random errors are addressed in the sensitivity analysis.

Systematic Errors

In general, the systematic errors were recognized, but no attempt to characterize them into a percent error of the measurement system was made. These errors are produced by approximating a physical occurance with an equation, or ignoring it. For example, the absorption of radiation by molecular oxygen was ignored since the effect is small for all but the lower altitudes of the rocket flights, as shown in Table 1. The doppler shift of radiation due to the motion of the rocket was also ignored, as it was shown to be smaller than the half width of the emission or absorption lines in Chapter II. The absorption profile is a doppler profile (Figure 2), while the emission profile becomes self-reversed as it propagates. The self-reversed emission profile has a minimum at the line center with increasing intensity toward the wings. It then is clear that the effect of doppler shifting the emission profile depends on the amount of self-reversal the emission profile has suffered, which depends on the distance from the rocket the source radiation has travelled. Self-reversal of the signal is also altitude dependent, since more self-reversal occurs for

the larger densities of the lower altitude region of the rocket flight for a given path length. Since the emission profile is usually broader than the absorption profile (see Figure 3), the wings of the emission profile lie outside the range of frequencies capable of being absorbed. For a severely self-reversed emission profile only the wings have non-zero intensities, and unless the emission profile is doppler shifted so that one wing lies inside the absorption frequency range, there will be no interaction. So the doppler shifting of the emission profile creates a varying effect that is not only dependent on the changing angle of the source emission to the RAM direction as the rocket spins, but also dependent on the distance the signal must travel before being resonantly scattered and returned to the rocket, and the altitude at which the measurement is made. These difficulties in accurately characterizing the effects of doppler shifting considered with the small value of the actual doppler shift, have convinced us that rigorous calculations of the changing role of the doppler shift are not worthwhile.

Flow effects near the rocket skin due to the supersonic speeds attained by sounding rockets definitely perturb the measurements, however these effects are difficult to assess. This is because of the turbulent environment existing in the wake of the rocket, and the unknown character of the wake, such as its size, and pressure and temperature perturbations. Figure 18 shows the modeled effects of the rocket wake assuming a horizontal component of motion. This simple model shows the effects averaging out over the spin period of the rocket. This may not be the actual case, especially since we ignore any contaminants outgassed by the rocket, and any temperature changes inside

inside the wake. The flow effects are also dependent on altitude, and thus present a difficult problem that was not dealt with. This was especially true for the Andoya flight, where the measurement region began at the rocket skin. Later flights excluded the region close to the rocket from being in the measurement region to minimize the flow effects.

Background contamination, both solar and auroral, increases the random noise of the system and degrades the quality of the measurement by increasing the random scatter of the data. This was in all cases ignored, except for the Eclipse flight in which an obvious solar contamination occured over the spin period of the rocket. The contaminated points were discarded. The Andoya flight data exhibited a contamination problem which severely limited the useful altitude range of the flight. This contamination was not understood (as discussed in Chapter V) and no attempts to remove it were made. As a result, the data exhibits a large scattering for much of the altitude profile (Figure 19).

The interaction between the radiation emitted by the source lamp and oxygen atoms has been characterized in an equation refered to in this paper as the effective microscopic cross section (see Chapter III). This term attempts to accurately describe the changing shape of the lamp emission profile as it propagates through the oxygen medium becoming self-reversed, and the amount of absorption it suffers along the way. As such it includes assumptions such as a doppler profile initially, a lamp characterized by a single temperature, and absorber atoms of constant temperature (at any one altitude). Also assumed is the mathematical formulation of the self-reversal of the propagating

signal. These assumptions obviously introduce some error to the final results, dependent on the accuracy of the assumptions. However, the degree of inaccuracy in the assumptions is a difficult question to answer, and so the errors introduced by using inaccurate equations are acknowledged but no attempt was made to evaluate their contribution to the total error.

Sensitivity Analyisis

The sensitivity analysis for the computer model was performed by using the sensitivity of the program to changes in any uncertain parameters. Only one parameter at a time was varied, and run through the model. This was repeated for each uncertain parameter, so that the individual error associated with each parameter change was found. This was necessary because some of the parameters occur in non-linear equations, and hence the error propagation was not obvious. Table 2 lists the fundamental uncertainties and the quantities used in the model that are affected by them. These quantities include the cross section of oxygen atoms to 130 nm radiation (σ_1), the optical depth ($k_0 l$), the effective normalized microscopic cross section (σ_2), the normalized transmission (T_{01}), the relative population densities of atoms in the three ground states (p(j)), the dimming of light due to off-axis viewing of the lamp (Dim), and geometry considerations.

From Table 2 it is easy to see that the emission and absorption temperatures propagate errors in more than one quantity. This complicates the consideration of errors due to uncertain temperature. It is helpful to examine individually the error propagation to the terms on the right side of Table 2, and then their effect on the final results

TABLE 2. Fundamental Uncertainties and the Quantities They Affect

Fundamental Uncertainties	Quantities affected
Emission Temperature	σ_1, $(k_0 l)$, σ_2, T_{01}
Absorption Temperature	σ_1, $(k_0 l)$, σ_2, T_{01}, $p(j)$
f value	σ_1, $(k_0 l)$
Dim	no other quantity affected
Geometry measurements	no other quantity affected

(the transfer function). Unfortunately the emission temperature in oxygen lamps is not a well known quantity. The model assumes a constant temperature of 900 K throughout the lamp. This has to be inaccurate since the walls of the lamp are certainly not at 900 K. One would expect a temperature profile, colder at the walls and increasing in temperature towards the lamp center electrode. The problem of temperature profile has been ignored, but the problem of uncertain lamp temperature can not be ignored. Lamp temperature uncertainty has been correlated in Table 3 and Table 4.

Table 3 shows the error produced in the normalized effective microscopic cross section (σ_2) and the normalized transmission (T_{01}) caused by uncertain lamp temperature. Since these errors are dependent on optical depth, they are each shown for three values of optical depth. The model uses optical depths from 0.0 to 19.5, although very little radiation penetrates to optical depths larger than 10. The effective cross section and transmission are also slightly dependent

on absorber temperature. Since an error of 4% occurs in these quantities for the largest reasonable variation in absorber temperature (Ta), Ta was not included in the table. Table 3 was calculated for an absorber temperature equal to 200 K. It is easily seen from Table 3 that lamp operation at lower temperatures has a more serious effect on the error than larger operation temperatures. One reason for attempting to provide large temperatures in the oxygen resonance lamps is to minimize errors due to uncertain lamp (and absorption) temperatures.

TABLE 3. Errors in σ_2 and T_{01} Due to Emission Temperature

Te	% change from 900 K	optical depth	$\Delta\sigma_2$	ΔT_{01}
500 K	44%	2.0	46%	19%
		5.0	59%	34%
		9.5	60%	43%
800 K	11%	2.0	8%	4%
		5.0	9%	7%
		9.5	10%	9%
1050 K	16%	2.0	9%	5%
		5.0	11%	9%
		9.5	11%	12%
1500 K	66%	2.0	28%	16%
		5.0	31%	30%
		9.5	32%	40%

From Table 3 it can be seen that deciding on the error contribution from effective cross section and transmission is quite a problem since it is very dependent on lamp temperature. Table 4 shows the

lamp temperature effects on the transfer function excluding the contribution of effective cross section and transmission. Here the emission temperature only affects σ_1, and through that the optical depth. Notice that the error is quite dependent on the density of the atomic oxygen being measured. Larger densities have larger errors associated with them. At densities of both 10^{12} and especially 10^{11} the second order scattering contributes less to the transfer function than first order scattering.

TABLE 4. Te Errors Excluding Effect on σ_2 and T_{01}

Te	% change from 900 K	first order error 10^{11}	first order error 10^{12}	second order error 10^{11}	second order error 10^{12}
500 K	44%	2-3%	16-23%	-	9-15%
800 K	11%	.6%	3-5%	-	-
1050 K	16%	.9%	4-6%	-	-
1500 K	66%	2-3%	15-18%	-	6-12%

Absorption temperature is also a quantity which contributes to the overall error. The cause of the error is quite different from that of the emission temperature. Emission temperature uncertainty is caused by imprecise knowledge of the lamp characteristics, whereas absorber temperature uncertainty is caused by uncertainty in knowledge of atmospheric temperature.

Since the atmospheric temperature data are stored in 1 km increments, and the largest variation of temperature from 1 km to the next was about 15 K, the interpolation of atmospheric temperature should be

within a 15 K limit of accuracy of the temperature data. Since the atmospheric temperature varies with altitude, the percent change in absorber temperature is listed in Table 5 over the atmospheric temperature range encountered in the 70 to 120 km altitude region. The percent change is listed for three different absorber temperature changes of 15 K, 10 K, and 5 K. Table 5 lists only the percent change in absorber temperature under different conditions, and not the percent error in the model caused by them. In all cases, the error caused by absorber temperature uncertainty was less than 1% (excluding the effect of Ta on σ_2 and T_{01}). This is certainly much less than the error caused by emission temperature uncertainty.

TABLE 5. Absorber Temperature Percent Error

Ta	15 K change	10 K change	5 K change
150 K	10.0%	7.5%	3.3%
200 K	7.5%	5.0%	2.5%
300 K	5.0%	3.3%	1.6%
400 K	3.7%	2.5%	1.2%

The calculation of optical depth is dependent upon the emission temperature, the absorption temperature, and the f value. The temperatures are square root dependent, and errors in them will result in a less extreme effect. The error produced in the calculation of optical depth will result in an error in both transmission and effective cross section, and hence the transfer function. Table 6 lists the error in

optical depth for assumed errors in the dependent quantities, and the effect on transmission and effective cross section. This is done for different values of optical depth, where again the larger values of optical depth are less important since not much light penetrates far into the medium. The error in transmission and effective cross section due to optical depth has already been included in the calculation of effective cross section and transmission errors due to temperature uncertainties, and f value uncertainty. It is interesting however to relate errors due to optical depth separately.

TABLE 6. Optical Depth ($k_0 l$) Effect on σ_2 and T_{01}

error cause	$\Delta(k_0 l)$	at value of ($k_0 l$)	$\Delta\sigma_2$	ΔT_{01}
Te (1150 K) - 28%		2	11%	8%
f value - 10%	17%	3	14%	9%
Ta - 5%		4	15%	11%

Now that the individual error associated with a change in any of the uncertain parameters has been found, they can be compared to each other to determine where the largest error to the system lies. The total error can also be calculated given the individual contributions to the error. The standard equation for total error is the square root of the sum of the squares of the individual errors. Table 7 lists the individual quantities producing errors, the assumed error of each, and the total error caused to the system for those assumptions.

An error in emission temperature causes an error in the transmission, effective cross section, and optical depth. Considering more than one error in emission temperature is useful since it is such an unknown quantity and has such drastic consequences on the results compared to other quantities. This is done at oxygen densities of 10^{11} and 10^{12} cm^{-3}, since the error can be dependent on density. Optical depth and population density errors are not in the table since their effect is included in Te, Ta, and the f value.

TABLE 7. Individual Contribution and Total Error

Quantity	Te ≈ 1500 K error at 10^{11}	Te ≈ 1500 K error at 10^{12}	Te ≈ 1100 K error at 10^{11}	Te ≈ 1100 K error at 10^{12}
σ_2	28%	28%	12%	12%
T_{01}	16%	16%	10%	10%
Te	3%	15%	1%	5%
Ta	0.1%	1%	0.1%	1%
f value	10%	10%	10%	10%
Dim	5%	5%	5%	5%
Geometry	2%	2%	2%	2%
Total error	34%	37%	19%	19%

The major error sources are from the calculated transmission of the signal, the calculated effective microscopic cross section (normalized overlap function), and f value. The error caused by using an incorrect emission temperature increases as optical depth increases, but becomes less important because the radiation is attenuated before reaching large optical depths. The individual contribution to the

error by the microscopic cross section varied between about 28 to 35% for the case of emission temperature equal to 1500 Kelvin (instead of 900 K used in the data reduction). For an emission temperature of 500 K the error was larger, varying between about 46 to 67%. The temperatures are probably more extreme than actual variations within the lamp, or from one lamp to the next [Rawlins and Kaufman, 1977]. The lamps used by USU operate between 5 and 7 Torr, and Rawlins and Kaufman give temperatures of 820 K plus or minus 30 K at 7 Torr, and 1000 K plus or minus 50 K at 4.5 Torr. There are, however, other parameters besides pressure which affect temperature in the lamp. The question of lamp temperature is still an unknown factor as evidenced by the increase of emission atom temperature with decreasing pressure. Rawlins and Kaufman attribute this to the dissociative excitation of O_2 by the $2s\,^1S$ state of helium, which is the dominant species in the lamp.

Both transmission and effective cross section errors occur because of their dependence on temperature and optical depth. The emission temperature contributes errors to the model in other places also. The errors associated with an error in absorbing temperature proved to be negligible (under 1%). Another major error (contributing a 10% individual error) encountered is the error in the atomic oxygen cross section to the 1304 Å radiation. This error comes from the uncertainty in the oscillator strength (f value) as derived in Chapter III. Other errors considered include the off-axis dimming of the lamp radiation, the convolution of the signal through an aperture, and measurements of the instrument configuration. The error in population density of absorbing atoms in the three ground states was included in

consideration of the absorbing temperature error. The fundamental causes of error were emission temperature, f value, absorbing temperature, and geometry measurements. All of the above assumes that the equations used give accurate results. This is probably the case for low optical depths. In this case the assumption of Continuous Frequency Redistribution (CFR) is valid [Strickland and Donahue, 1970]. CFR assumes that the emission frequency of a photon by an absorbing atom is independent of the absorbed photon frequency. However as the oxygen density increases above 10^{11} this assumption becomes questionable.

The standard deviation of the measured counts per second was quite small. When averaging over 1 km distances, the largest standard deviation was about 40 counts per second out of a count rate of about 10^6 counts per second at the peak density for the Tracer flight. This is very much smaller than any of the other errors considered. This indicates that the structure measured by the system should be quite believable. The total error found in the model by varying uncertain parameters depended on the oxygen density, and the emission temperature. For large emission temperature variation (Te ≈ 1500 K) at densities of 10^{11} cm^{-3} an error of about 34% was found. A density of 10^{12} gave an error of about 37%. For less extreme emission temperature variation (Te ≈ 1100 K) an error of about 19% was found for both densities. Then assuming that our lamp temperature does not vary by much more than the ones which Rawlins and Kaufman reported (probably a reasonable assumption), and also assuming that our modeled equations are accurate, the total error of this measurement system would be 20%.

CHAPTER VII

CONCLUSION

In conclusion, the resonant scatter technique provides a good means of measuring atomic oxygen densities near the peak density altitude (70 to 120 km). Using the scattering of light allows measurement of the oxygen atoms without having to bring them into the instrument. The only real disturbance of the atoms is caused by the wake of the supersonic rocket. At the small pressure of the upper atmosphere this is thought not to be a major effect, although the disturbed atoms near the rocket will introduce an error to the model, which considers constant density and temperature only.

The photodissociation of O_2 at altitudes below 80 km is also a concern, since it artificially creates more oxygen atoms from the lamp emission radiation. The effect of this is unclear, since in producing more oxygen atoms, lamp emission photons are lost. This is a negligible effect over the region of the peak density, where the resonant scatter technique performs quite well as a measurement system for atomic oxygen densities. The greatest advantage of the resonant scatter measurement is the great speed at which the signal is returned. This allows a good spatial resolution of less than a tenth of a kilometer. Although averaging over smaller distances is possible, the random scattering of the data increases, sometimes making the reduction less desirable.

Another factor contributing to the sensitivity is the independence of the measurement from assumed models of production and quenching mechanisms, and the associated rate constants. This also contri-

butes to the reliability of structure measured. It has been seen in the past that the shape of the oxygen density profile measured by in situ devices can differ substantially from the profile predicted using 5577 Å measurement devices which require the use of these rate constants in the production and quenching models [Philbrick et al., 1974].

The ability of the system to measure absolute densities seems good, but without the support of a calibration to the system, the data can only be compared to other measurement techniques as to the validity measurement system. The combination of resolution (which is unsurpassed by any other system) and absolute measurement ability makes the resonant scatter technique one to be recommended highly for measurements near the peak density, especially when observation of structure is of interest.

The single most important quantity to the use of a computer model to evaluate oxygen density by the resonant scatter technique is the emission temperature in the lamp. This temperature needs to be evaluated in detail, and attempts to accurately measure this temperature should be considered. The emission temperature is crucial in determining the emission frequency profile of the lamp, along with other lamp operating parameters such as pressure. The fine resolution measurement of the emission frequency profile of each of the three lines is the ultimate goal, and would bypass the need for knowledge of the lamp temperature. Measurement of the line shapes could be achieved by use of an echelle grating with very fine resolution. A discussion of echelle gratings and appropriate mounting devices can be found in Samson [1967]. Dickinson et al., [1980] reports on the use of the 1.5 m

Photoelectric Echelle Spectrograph at the Division of Quantum Metrology at the National Physical Laboratory in Teddington, England, to obtain a wavelength resolution of 0.004 Å for the triplet of 130 nm.

The oscillator strength for the resonant transition has been measured in the past, and hopefully future measurements will give less than a 10% error. The dimming of light from the lamp due to being off the lamp axis should be measured for each lamp before flight. This should be done over the entire angular range encountered by the model (about 12 degrees), as this profile does not seem to be linear as expected. This was done only for the Tracer flight. One final recommendation to be made is for the calibration of the model using a known quantity of oxygen as a reference. This is of course not a simple task, but would yield extremely useful information. The difficulty of addressing the absolute error of the computer model lies with the unknown degree to which the model characterizes our measurement system. With a calibration of the system and the measurement of the emission frequency profile, the absolute measurement capability of the resonant scatter technique would greatly improve, and confidence in the system would be achieved. A reduction of the model's sensitivity to parameter changes to about 12% would be the result, yielding higher accuracy along with the fine resolution of the measurement system over the peak density region. Since the measurement of the emission profile and calibration are both possible with present technology, the resonant scatter technique promises to be an excellent in situ measurement system for atomic oxygen at the peak density altitude range.

REFERENCES

Anderson, D. E., Jr., R. R. Meier, P. D. Feldman, E. P. Gentieu, The UV dayglow 3, OI emissions at 989, 1027, 1152, 1304, 1356 angstrom, Geophysical Research Letters, 7, 1057-1060, 1980.

Baker, K. D., D. A. Burt, R. D. Harris, L. C. Howlett, L. C. Jenson, W. R. Pendleton, E. F. Pound, G. D. Allred, Rocket measurements of D- and E-region parameters during the 26 february 1979 total eclipse, Physical Sciences Lab., Las Cruces, New Mexico, 1980.

Dickinson, P. H. G., W. C. Bain, L. Thomas, E. R. Williams, D. B. Jenkins, N. D. Twiddy, The determination of the atomic oxygen concentration and associated parameters in the lower ionosphere, Proc. Roy. Soc. London, A369, 379-408, 1980.

Dickinson, P. H. G., N. D. Twiddy, R. A. Young, Atomic oxygen concentrations in the lower ionosphere, Space Res., XVI, 301-305, 1976.

Donahue, T. M., B. Guenther, R. J. Thomas, Distribution of atomic oxygen in the upper atmosphere deduced from Ogo 6 airglow observations, J. Geophys. Res., 78, 6663-6689,1973.

Donahue, T. M., B. Guenther, Comment on 'Atomic oxygen densities in the lower thermosphere as derived from in situ 5577 angstrom night airglow and mass spectrometer measurements', J. Geophys. Res., 80, 219-220, 1975.

Donahue, T. M., D. J. Strickland, Excitation and radiative transport of OI 1304 angstrom resonance radiation - II The aurora, Planet. Space Sci., 18, 691-697, 1970.

Dyson, P. L., G. P. Newton, L. H. Brace, In situ measurements of neutral and electron density wave structure from the Explorer 32 satellite, J. Geophys. Res., 75, 3200-3210, 1970.

Fastie, W. G., H. M. Crosswhite, D. F. Heath, Rocket spectrophotometer airglow measurements in the far ultraviolet, J. Geophys. Res., 69, 4129-4140, 1964.

Forbes, J. M., F. A. Marcos, Seasonal-Latitudinal tidal structures of O, N_2, and total mass density in the thermosphere, J. Geophys. Res., 85, 3489-3493, 1980.

Georges, T. M., HF doppler studies of traveling ionospheric disturbances, J. Atmos. Terr. Phys., 30, 735-746, 1968.

Golomb D., R. E. Good, Atomic oxygen profiles over Churchill and Hawaii from chemical releases, Space Res., XII, 675-683, 1972.

Hedin, A. E., C. A. Reber, G. P. Newton, N. W. Spencer, H. C. Brinton, H. G. Mayr, W. E. Potter, A global thermospheric model based on mass spectrometer and incoherent scatter data MSIS 2. Composition, J. Geophys. Res., 82, 2148-2156, 1977.

Henderson, W. R., Atomic oxygen profile measurements, J. Geophys. Res., 79, 3819-3826, 1974.

Howlett, L. C., K. D. Baker, Development of a rocket-borne resonance lamp system for the measurement of atomic oxygen, Rep. AFGL-TR-77-0227, Air Force Geophys. Lab., Bedford, Mass., 1977.

Hudson, R. D., Critical review of ultraviolet photoabsorption cross sections for molecules of astrophysical and aeronomic interest, Rev. Geophys. Space Phys., 9, 305-406, 1971.

Imbro, D. R., M. M. Moe, K. Moe, On fundemental problems in the deduction of atmospheric densities from satellite drag, J. Geophys. Res., 80, 3077-3086, 1975.

Lake, L. R., A. O. Nier, Loss of atomic oxygen in mass spectrometer ion sources, J. Geophys. Res., 78, 1645-1653, 1973.

Lawrence, G. M., Vacuum ultraviolet transition probabilities in C, N, O, and N_2, Canadian Journal of Chemistry, 47, 1856-1857, 1969.

Lee, P., Photodissociation and photoionization of oxygen (O_2) as inferred from measured absorption coefficients, J. Opt. Soc. Am., 45, 703-709, 1955.

McEwan, M. J., L. F. Phillips, Chemistry of the Atmosphere, 301 pp., Wiley, New York, 1975.

Meier, R. R., Jong-sen Lee, An analysis of the 1304 angstrom dayglow using a Monte Carlo resonant scatter model with a partial frequency redistribution, Planet. Space Sci., 30, 439-450, 1982.

Mitchell, A. C. G., M. W. Zemansky, Resonance Radiation and Excited Atoms, 338 pp., Cambridge, New York, 1961.

Newton, G. P., D. T. Pelz, H. Volland, Direct in situ measurements of wave propogation in the neutral thermosphere, J. Geophys. Res., 74, 183-196, 1969.

Nier, A. O., W. E. Potter, D. C. Kayser, Atomic and molecular oxygen densities in the lower thermosphere, J. Geophys. Res., 81, 17-24, 1976.

Offermann, D., A. Drescher, Atomic oxygen densities in the lower thermosphere as derived from in situ 5577 angstrom night airglow and mass spectrometer measurements, J. Geophys. Res., 78, 6690-6700, 1973.

Offermann, D., A. Drescher, Reply, J. Geophys. Res., 80, 221-222, 1975.

Offermann, D., H. Trinks, A rocket borne mass spectrometer with heliun cooled ion source, Review of Scientific Instruments, 42, 1836-1843, 1971.

Penndorf, R., Tables for the refractive index for standard air and the Rayleigh scattering coefficient for the spectral region between 0.2 and 20.0 μ and their application to atmospheric optics, Journal of the Optical Society of America, 47, 176-182, 1957.

Perov, S. P., A. S. Rakhmanov, Atomic oxygen concentration measurements by a rocket near the mesopause, Space Res., XVII, 261-264, 1977.

Philbrick, C. R., G. A. Faucher, E. Trzcinski, Rocket measurements of mesospheric and lower thermospheric composition, Space Res., XIII, 255-260, 1973.

Philbrick, C. R., D. Golomb, S. P. Zimmerman, T. J. Keneshea, M. A. MacLeod, R. E. Good, B. S. Dandekar, B. W. Reinisch, The ALADDIN II experiment: Part II, Composition, Space Res., XIV, 89-95, 1974.

Pokhunkov, A. A., Mass-spectrometer investigation of upper atmosphere neutral composition at equatorial, middle, and polar latitudes, Space Res., XII, 657-663, 1972.

Rawlins, W. T., F. Kaufman, Characteristics of O(I) and N(I) resonance line broadening in low pressure helium discharge lamps, Journal of Quantitative Spectroscopy and Radiative Transfer, 18, 561-572, 1977.

Reber, C. A., A. E. Hedin, D. T. Pelz, W. E. Potter, L. H. Brace, Phase and amplitude relationships of wave structure observed in the lower thermosphere, J. Geophys. Res., 80, 4576-4580, 1975.

Samson, J. A. R., Techniques of Vacuum Ultraviolet Spectroscopy, 348 pp., Wiley, New York, 1967.

Scholz, T. G., D. Offermann, Measurement of neutral atmospheric composition at 85 - 150 km by mass spectrometer with cryroion source, J. Geophys. Res., 79, 307-310, 1974.

Strickland, D. J., T. M. Donahue, Excitation and radiative transport of OI 1304 angstrom resonance radiation - I The dayglow, Planet. Space Sci., 18, 661-689, 1970.

Strickland, D. J., M. H. Rees, The OI λ1304 and λ1356 emissions in aurorae, Planet. Space Sci., 22, 465-481, 1974.

Tanaka, Y., E. C. Y. Inn, K. Watanabe, Absorption coefficients of gases in the vacuum ultraviolet, IV. Ozone, Journal of Chemical Physics, 21, 1651-1653, 1953.

Thomas, R. J., D. J. Baker, Silver film atomic oxygen sensors, Canadian Journal of Physics, 50, 1676-1681, 1972.

Trinks, H., D. Offermann, U. von Zahn, C. Steinhauer, Neutral composition measurements between 90- and 220-km altitude by rocket-borne mass spectrometer, J. Geophys. Res., 83, 2169-2176, 1978.

von Zahn, U., Measurements of atomic oxygen in the upper atmosphere: A critical review, J. Geophys. Res., 72, 5933-5937, 1967.

von Zahn, U., Neutral air density and composition at 150 kilometers, J. Geophys. Res., 75, 5517-5527, 1970.

Wasser, B., T. M. Donahue, Atomic oxygen between 80 and 120 km: Evidence for a latitudinal variation in vertical transport near the mesopause, J. Geophys. Res., 84, 1297-1309, 1979.

Watanabe, K., F. F. Marmo, Photoionization and total absorption cross sections of gases. II. O_2 and N_2 in the region 850-1500 A, Journal of Chemical Physics, 25, 965-971, 1956.

Watanabe, K., F. M. Matsunaga, H. Sakai, Absorption coefficient and photoionization yield of NO in the region 580-1350 A, Applied Optics, 6, 391-396, 1967.

APPENDIX

```
            PROGRAM ATTEN
C
C THIS PROGRAM CALCULATES THE NORMALIZED ATTENUATION OF LIGHT AS A
C FUNCTION OF OPTICAL DEPTH, WITH ABSORBER TEMPERATURE AS A
C PARAMETER.
C                              J.ELWELL    4/13/80
C    REVISED 6/2/80               J.ELWELL
C    REVISED 9/22/80              J.ELWELL
C
     REAL ATEN(40),W,NUM,DEN,OD,AB,A
C RECORDS IN THIS FILE ARE 164 BYTES LONG, SO SET THE
C OPTION MAXBUF TO THIS VALUE WHEN LINKING.
     OPEN(UNIT=1,NAME='DATTEN.DAT',TYPE='NEW',ACCESS='DIRECT'
      +,RECORDSIZE=41)
C
C THE OPTICAL DEPTH IS VARIED FROM 0 TO 19.5 IN .5 INCREMENTS,
C AND THE INTEGRATION IS PERFORMED WITH OMEGA (W) VARYING FROM
C -10 TO +10 IN .1 INCREMENTS. THIS IS DONE 9 TIMES, FOR ABSORBER
C TEMPERATURES OF 200K TO 1000K IN 100K INCREMENTS.
C
C    STATEMENT OF VARIABLES
C
C    ATEN     ATTENUATION
C    W        OMEGA (FREQUENCY)
C    NUM      NUMERATOR
C    DEN      DENOMINATOR
C    OD       OPTICAL DEPTH
C    AB       ABSORBER TEMPERATURE
C    A        ALPHA
C
C INDEX AB WILL GO THROUGH THE ABSORBER TEMPERATURES.
     DO 7 AB=200.,1000.,100.
C ALPHA=SQRT(EMITTER TEMPERATURE/ABSORBER TEMPERATURE)
     A=SQRT(900./AB)
C THE DENOMINATOR OF THIS IS CONSTANT FOR ANY ABSORBER
C TEMPERATURE SO CALCULATE IT NOW.
     DEN=0.
     DO 8 W=-10.,10.,.1
     DEN=DEN+EXP(-(W/A)**2)*.1
   8 CONTINUE
C NOW WE CALCULATE THE ATTENUATION AT EACH OPTICAL DEPTH,
C AND NORMALIZE.
     DO 9 OD=0.,19.5,.5
     IND=(OD+.5)*2
C NOW INTEGRATE THROUGH THE FREQUENCY.
     NUM=0.
     DO 10 W=-10.,10.,.1
     NUM=NUM+EXP(-(W/A)**2-OD*EXP(-W**2))*.1
  10         CONTINUE
C NOW CALCULATE THE ATENUATION, AND SAVE IT.
     ATEN(IND)=NUM/DEN
C GO DO THE NEXT DEPTH.
   9 CONTINUE
```

```
C WRITE RESULTS TO USER AND DISK.
      IREC=(AB/100.)-1
      WRITE(1'IREC) AB,ATEN
      WRITE(5,2)AB,ATEN
    2 FORMAT(' ABTMP=',F5.0,8(/1X,5(F10.8,2X)))
C GO DO THE NEXT TEMPRATURE.
    7 CONTINUE
C ALL DONE!
      CLOSE(UNIT=1)
      STOP'THE VERY END'
      END
```

```
      PROGRAM SIGMA
C
C     CALCULATES  EFFECTIVE CROSS SECTION OF
C  ATOMIC OXYGEN AS A FUNCTION OF OPTICAL DEPTH,
C  WITH ABSORBER TEMPERATURE AS A PARAMETER.
C                       J.ELWELL   4/12/80
C      REVISED 6/2/80  J.ELWELL
C      REVISED 9/22/80 J.ELWELL
C
      REAL SGMA(40),W,NUM,DEN,OD,AB,A,TMP
C  RECORDS IN THIS FILE ARE 164 BYTES LONG, SO SET THE
C  OPTION MAXBUF TO THIS VALUE WHEN LINKING.
C
      OPEN(UNIT=1,NAME='DSIGMA.DAT',TYPE='NEW',ACCESS='DIRECT'
     +,RECORDSIZE=41)
C
C  THE OPTICAL DEPTH WILL GO FROM 0 TO 19.5 IN .5
C  INCREMENTS. THE ABSORBER TEMPERATURE WILL GO FROM
C  200K TO 1000K IN 100K INCREMENTS. THE EQUATIONS WILL BE
C  INTEGRATED OVER AN OMEGA OF -10 TO 10 IN .1 INCREMENTS.
C  AN EMITTER TEMPERATURE OF 900K IS ASSUMED.
C
C           STATEMENT OF VARIABLES
C
C        SGMA          EFFECTIVE CROSS SECTION
C        W             OMEGA (FREQUENCY)
C        NUM           NUMERATOR
C        DEN           DENOMINATOR
C        OD            OPTICAL DEPTH
C        AB            ABSORBER TEMPERATURE
C        A             ALPHA
C        TMP           TEMPORARY
C
C  INDEX AB WILL GO THROUGH THE ABSORBER TEMPERATURES.
      DO 7 AB=200.,1000.,100.
C  ALPHA=SQRT(EMITTER TEMPERATURE/ABSORBER TEMPERATURE)
      A=SQRT(900./AB)
C  INDEX OD WILL STEP THROUGH THE OPTICAL DEPTH.
      DO 8 OD=0.,19.5,.5
      NUM=0.
      DEN=0.
C  INDEX W WILL STEP THROUGH THE FREQUENCY AND THE INTEGRATION
C  WILL BE DONE.
      DO 9 W=-10.,10.,.1
C  CALCULATE A COMMON TERM.
      TMP=EXP(-(W/A)**2-OD*EXP(-W**2))*.1
      NUM=NUM+TMP*EXP(-W**2)
      DEN=DEN+TMP
    9 CONTINUE
C  FIND WHERE TO PUT IT, AND SAVE SIGMA.
      IND=OD*2.+1.
      SGMA(IND)=NUM/DEN
    8 CONTINUE
```

```
C NOW PRINT RESULTS TO USER AND DISK.
      IREC=(AB/100.)-1
      WRITE(1'IREC) AB,SGMA
      WRITE(5,2)AB,SGMA
    2 FORMAT(' ABTMP=',F5.0,8(/1X,5(F10.8,2X)))
    7 CONTINUE
C ALL DONE!
      CLOSE(UNIT=1)
      STOP'THE VERY END'
      END
```

```
      PROGRAM GSCAT
C
C THIS PROGRAM GENERATES THE DATA, FOR A GIVEN INSTRUMENT GEOMETRY,
C NECESSARY TO RUN THE SECOND ORDER SCATTERING PROGRAM.
C                                        J.ELWELL   6/4/80
C
C   REVISED  9/22/80   J.ELWELL
C
C
C   STATEMENT OF VARIABLES
C
C   DA       AREA OF DETECTOR
C   DAR      RADIUS OF DETECTOR APERTURE
C   DB       DISTANCE FROM SOURCE POINT TO DISK BOTTOM RADIUS
C   DD       DISTANCE FROM ROCKET SKIN TO DETECTOR DISK
C   DIN1     DISTANCE FROM DETECTOR TO ROCKET SKIN
C   DIN2     LENGTH FROM MIN ANGLE MEETS AXIS TO ROCKET SKIN
C   DR       RADIUS OF DETECTOR
C   DS       DISTANCE BETWEEN DETECTOR AND DETECTOR APERTURE
C   DST      DISTANCE BETWEEN SOURCE POINT AND DETECTOR DISK
C   DT       DISTANCE FROM SOURCE POINT TO DISK TOP RADIUS
C   DX       X COMPONENT OF DS
C   DY       Y COMPONENT OF DS
C   GEO      INSTRUMENT GEOMETRY IDENTIFIER
C   PHI      ANGLE BETWEEN SOURCE AND DETECTOR AXIS
C   PHIC     COS(PHI)
C   PHIS     SIN(PHI)
C   PI       3.14159
C   RAD      RADIUS OF DETECTOR DISK
C   RADI     INNER RADIUS OF DETECTOR DISK
C   RAT      RATIO OF DETECTOR AREA TO AREA OF COMPLETE SPHERE
C   RX       X COMPONENT OF RADI
C   RY       Y COMPONENT OF RADI
C   SQRT     SQRT(2)
C   SX       X DISTANCE OF SOURCE POINT
C   TANA     TANGENT OF DETECTOR CONE MINIMUM ANGLE
C   VOL      VOLUME OF EACH DETECTOR DISK
C   XO       LENGTH OF SOURCE AXIS FROM ROCKET TO DETECTOR AXIS
C   X*       X1,X2,....;DUMMY VARIABLES
C   YO       LENGTH FROM WHERE SOURCE AND DETECTOR AXIS EXIT ROCKET
C
C
      REAL DST(100),VOL(100),RAT(100)
      BYTE GEO(11)
C
      PARAMETER PI=3.14159,SQRT2=1.4142
C
      DATA GEO/'D','S',4*0,'.','D','A','T',0/
C
C LINK WITH THIS OPTION:
C LINK/OPTIONS GSCAT
C MAXBUF=400
C /
```

```
C
C UNIT DEFINITIONS:
C    1-INSTRUMENT SPECIFICATIONS (INPUT) (NAME: DS----.DAT)
C    2-COMPUTED DATA (OUTPUT) (NAME: DI----.DAT)
C
     TYPE*,'ENTER FOUR LETTER GEOMETRY IDENTIFIER.'
     ACCEPT6, (GEO(K),K=3,6)
   6         FORMAT(4A1)
C
     OPEN(UNIT=1,NAME=GEO,TYPE='OLD')
     GEO(2)='I'
     OPEN(UNIT=2,NAME=GEO,TYPE='NEW',ACCESS='DIRECT'
      +,RECORDSIZE=100)
C
C GET INSTRUMENT SPECIFICATIONS.
     READ(1,*) X1,X2,X3,X4
     READ(1,*) X1,X2,X3,X4
     READ(1,*) X1,X2,X3,X4
     READ(1,*) DR,DAR,DS,DIN1
     READ(1,*) X1,X2,X3,DIN2
     READ(1,*) X1,X2,X3,X4
     READ(1,*) XO,YO,PHI
C CALCULATE NEEDED CONSTANTS.
     TANA=(DAR-DR)/DS
     DA=PI*DR**2
     PHIC=COS(PHI)
     PHIS=SIN(PHI)
C
C THIS NEXT LOOP STEPS THROUGH THE 10 SOURCE POINTS.  EACH TIME
C THROUGH THE DISTANCE TO THE 100 DETECTOR DISKS WILL BE CALCULATED.
C THE FIRST TIME ONLY, THE VOLUME AND RATIO DATA WILL BE CALCULATED.
     DO 7 I=1,10
C FIND THE X DISTANCE OF THE SOURCE POINT.
     SX=FLOAT(I)-.5
C NOW THROUGH THE DETECTOR DISKS.
     DO 8 J=1,100
C FIND THE DETECTOR DISTANCE AND X AND Y COMPONENTS.
     DD=FLOAT(J)-.5
     DX=PHIC*DD
     DY=PHIS*DD
C FIND THE RADIUS OF THE DETECTOR DISK.
     RAD=TANA*(DD+DIN2)
C WE ONLY NEED TO CALCULATE VOLUME AND RATIO DATA ONCE.
     IF(I.NE.1)GOTO 10
C FIND THE VOLUME OF THIS DISK.
     VOL(J)=PI*RAD**2
C FIND THE RATIO OF DETECTOR AREA TO THE AREA OF A COMPLETE SPHERE.
     RAT(J)=DA/(4.*PI*(DD+DIN1)**2)
C NOW FIND THE DISTANCE BETWEEN THE SOURCE POINT AND THE DETECTOR
C DISK.  USE THE AVERAGE DISTANCE FROM THE SOURCE POINT TO THE
C "INNER RADIUS" OF THE DISK.
C FIND INNER RADIUS.
   10        RADI=RAD*SQRT2
```

```
C THIS HAS AN X AND A Y COMPONENT.
    RX=RADI*PHIS
    RY=RADI*PHIC
C NOW THE DISTANCE TO THE TOP AND BOTTOM OF THE INNER RADIUS.
    DT=SQRT((SX-DX+RX)**2+(DY+RY)**2)
    DB=SQRT((SX-DX-RX)**2+(DY-RY)**2)
C WE WANT THE MEAN OF THESE TWO.
    DST(J)=(DT+DB)/2.
    8       CONTINUE
C PUT RESULTS ON DISK.  FIRST TIME ONLY FOR VOLUME AND RATIO DATA.
    WRITE(2'I) DST
    TYPE*,'DST',I,DST
    IF(I.NE.1) GOTO 7
    WRITE(2'11) VOL
    TYPE*,'VOL',VOL
    WRITE(2'12) RAT
    TYPE*,'RAT',RAT
C GO DO ANOTHER SOURCE POINT.
    7       CONTINUE
C ALL DONE!!!!!!!!!!!!!!!!!!!!!!!!!
    CLOSE(UNIT=1)
    CLOSE(UNIT=2)
    STOP'THE VERY END'
    END
```

```
      PROGRAM SCAT
C
C THIS PROGRAM CALCULATES THE SECOND ORDER SCATTERING
C OF ATOMIC OXYGEN.
C                              J.K.ELWELL   6/4/80
C
C   REVISED 9/22/80   J.ELWELL
C
C
C ****** REVISED TO INCLUDE THE POSSIBILITY OF RECTANGULAR APERTURES
 *****
C                               4/15/82   NEIL MYERS
C
C THIS PROGRAM SHOULD BE LINKED AS FOLLOWS:
C LINK/OPTIONS SCAT
C MAXBUF=400
C ACTFIL=7
C UNITS=7
C /
C
C   STATEMENT OF VARIABLES
C
C   ABTMP   TEMPERATURE OF ABSORBING MEDIUM
C   ATOUT   ATTENUATION OUT FROM SOURCE TO ABSORBER
C   ATTEN   ARRAY GIVING ATTENUATION VS. OPTICAL DEPTH
C   AT2     ATTENUATION AT PREVIOUS DISK
C   CLC     CALCULATED LINE CONSTANTS
C       CONF    GEOMETRY CONFIGURATION (CONF=1 MEANS RECTANGULAR
 APERTURES)
C   DST     DISTANCE BETWEEN SOURCE POINT AND DETECTOR DISK
C   EANG    ANGLE AT WHICH EMITTER (LAMP) OUTPUT IS ZERO
C   ETMP    EMITTER (LAMP) TEMPERATURE
C   FLUX    ARRAY GIVING ABSORBED FLUX AT EACH SOURCE DISK
C   GEO     INSTRUMENT GEOMETRY IDENTIFIER
C   IND     OPTICAL DEPTH INDEX
C   IREC    POINTS TO DIRECT ACCESS RECORDS
C   OD      OPTICAL DEPTH
C       OX      OXYGEN DENSITY
C   PI      3.14159
C   POD     PRELIMINARY OPTICAL DEPTH
C   RAT     RATIO OF DETECTOR AREA TO AREA OF COMPLETE SPHERE
C   RATIO   RATIO OF ABSORBER AREA TO AREA OF COMPLETE SPHERE
C       SAL     SOURCE APERTURE LENGTH (FOR RECTANGULAR APERTURES)
C   SAR      SOURCE APERTURE RADIUS
C   SAVG    AVERAGE FLUX FROM SOURCE OVER SOURCE MIN ANGLE
C   SDSK    FLUX ABSORBED IN A DETECTOR DISK
C   SINT    SOURCE PEAK INTENSITY
C   SINTNS  SOURCE INTENSITY FOR EACH LINE (PHOTONS/SEC-SR)
C   SMIN    UNOCCLUDED ANGLE OF SOURCE
C       SMINL   SAME AS SMIN, BUT FOR RECTANGULAR APERTURE LENGTH
C   SMO     MINIMUM FLUX FROM SOURCE OVER SOURCE MIN ANGLE
C       SMO1    SAME AS SMO, BUT FOR SMINL AS MINIMUM ANGLE.
C   SR      SOURCE RADIUS
```

```
C   SS       DISTANCE BETWEEN SOURCE AND SOURCE APERTURE
C   SSLD     SOLID ANGLE CORROSPONDING TO SOURCE MIN ANGLE
C   STOT     TOTAL PHOTONS/SEC IN SOURCE CONE (TO MIN ANGLE)
C   TOT      TOTAL DETECTED FLUX FOR 100 DETECTOR DISKS
C   TOTAL    TOTAL DETECTED FLUX
C   TOT2     TOTAL DETECTED FLUX FOR 100 DISKS AND 10 SOURCES
C   TYP      TYPE OF DATA: 0-STOP,1-DENSITY,2-TEMPERATURE
C   VOL      VOLUME OF EACH DETECTOR DISK
C   XSECTN   MICROSCOPIC CROSS SECTION
C   X*       X1,X1,X3,.....;DUMMY VARIABLES
C   ZGMA0    SIGMA0
C   ZIGMA    ARRAY GIVING EFFECTIVE CROSS SECTION VS. OPTICAL DEPTH
C
C
    REAL VOL(100),CLC(3),FLUX(3,10),DST(100),ZIGMA(40)
    REAL ATTEN(40),SINTNS(3),RAT(100),XLN(3)
    BYTE GEO(11)
C
    PARAMETER PI=3.14159,ETMP=900.,SINT=1.E13,EANG=.5585
C
    DATA GEO/'D','S',4*0,'.','D','A','T',0/
C
C UNIT DEFINITIONS:
C     6-RUN CONTROL AND TEMPERATURE DATA
C     2-SPECIFICATIONS OF INSTRUMENT
C     3-OUTPUT CALCULATED RESULTS
C     4-CROSS SECTION VS. OPTICAL DEPTH DATA
C     5-TERMINAL
C     1-GENERATED MODEL SPECIFICATIONS
C     7-ATTENUATION VS. OPTICAL DEPTH DATA
C
    TYPE*,'ENTER FOUR LETTER INSTRUMENT GEOMETRY IDENTIFIER.'
    ACCEPT6, (GEO(K),K=3,6)
    6       FORMAT(4A1)
C
    OPEN(UNIT=6,NAME='DB0:DINDAT.DAT',TYPE='OLD')
    OPEN(UNIT=2,NAME=GEO,TYPE='OLD')
    GEO(2)='2'
    OPEN(UNIT=3,NAME=GEO,TYPE='NEW')
    OPEN(UNIT=4,NAME='DSIGMA.DAT',TYPE='OLD',ACCESS='DIRECT')
    GEO(2)='I'
    OPEN(UNIT=1,NAME=GEO,TYPE='OLD',ACCESS='DIRECT')
    OPEN(UNIT=7,NAME='DB0:DATTEN.DAT',TYPE='OLD',ACCESS='DIRECT')
C
C
C THE FOLLOWING SPECIFICATIONS COMPLETELY DEFINE
C THE GEOMETRY OF THE INSTRUMENT.
    READ(2,*) SR,SAR,SS,X1
        READ(2,*) X1,X2,X3,X4
        READ(2,*) X1,X2,X3,X4
        READ(2,*) X1,X2,X3,X4
        READ(2,*) X1,X2,X3,X4
        READ(2,*) X1,X2,X3,X4
```

```
        READ(2,*) X1,X2,X3
        READ(2,*) SAL,X1,X2,CONF
C
C THE METHOD:  THE SOURCE CONE IS DIVIDED INTO 10 1-CM THICK DISKS
 THAT
C BEGIN WHERE THE CONE LEAVES THE ROCKET.  THE FLUX ABSORBED BY EACH
C DISK IS CALCULATED.  THIS FLUX IS THE RE-RADIATED FROM EACH SOURCE
C DISK AND ACTS LIKE A SOURCE FOR EACH OF 100 DETECTOR DISKS.  THE
 FLUX
C ABSORBED BY EACH DETECTOR DISK FROM EACH SOURCE IS CALCULATED.  EACH
C DETECTOR DISK THEN ACTS AS A SOURCE FOR THE DETECTOR, AND THE FLUX
C EACH DETECTOR DISK CONTRIBUTES TO THE DETECTOR IS COMPUTED.
C
C FIRST, CALCULATE THE INTENSITY IN EACH OF 3 LINES IN THE UNOCCULTED
C SOURCE CONE.  ASSUMPTIONS:  A PEAK INTENSITY OF SINT=1.E13
C PHOTONS/SEC-SR ON THE AXIS OF THE LAMP;  THE OUTPUT LINEARLY DROPS
C TO ZERO AT AN ANGLE OF EANG=.5585;  LINE RATIOS FOR THE LAMP ARE
C 1:2.7:4.3.
C
C FIND THE UNOCCULTED SOURCE ANGLE, AND THE CORROSPONDING SOLID ANGLE.
    SMIN=ATAN((SAR-SR)/SS)
C FIND THE OUTPUT AT THE ANGLE SMIN.
        SMO=SINT*(EANG-SMIN)/EANG
C MAKE A DECISION HERE.  IS THE APERTURE GEOMETRY CIRCULAR OR
C  RECTANGULAR. 'CONF'=1 MEANS RECTANGULAR.
        IF(CONF.EQ.1)GOTO 22
C FOR CIRCULAR APERTURES:
    SSLD=2.*PI*(1.-COS(SMIN))
C FIND THE AVERAGE OUTPUT IN PHOTONS/SEC-SR FROM 0 TO SMIN.
    SAVG=(SINT+SMO)/2.
        GOTO 23
C FOR RECTANGULAR APERTURES:
C
  22    SMINL=ATAN((SAL-SR)/SS)
C SOLID ANGLE IS AREA/(RADIUS SQUARED).
        SSLD=2*SAL*SAR/SS**2
C FIND THE AVERAGE OUTPUT IN PHOTONS/SEC-SR FOR THE LENGTH OF THE
 APERTURE.
C  FOR GEO6 THE LAMP WAS FOUND TO PEAK OFF AXIS AT .1745 RADIANS, WITH
C A PEAK OF 1.115 (NORMALIZED TO ONE ON THE AXIS), WITH AN ASSUMED
C LINEAR DROP TO ZERO AT EANG(.5585).
        IF(SMIN.LE..1745)DIM=(.115/.1745)*SMIN+1.
        IF(SMIN.GT..1745)DIM=-(1.115/(EANG-.1745))*(SMIN-.1745)+1.115
        SMO=SINT*DIM
        IF(SMINL.LE..1745)DIML=(.115/.1745)*SMINL+1.

 IF(SMINL.GT..1745)DIML=-(1.115/(EANG-.1745))*(SMINL-.1745)+1.115
        SMO1= SINT*DIML
C THE AVERAGE OUTPUT OVER THE RECTANGLE IS APRROXIMATELY THE AVERAGE
C OF THE LENGTH AND WIDTH AVERAGES.
        SAVG=((SINT+SMO) + (SINT+SMO1))/4.
  23    CONTINUE
C THIS AVERAGE TIMES THE ACTUAL SOLID ANGLE GIVES PHOTONS/SEC.
```

```
      STOT=SAVG*SSLD
C DIVIDE THIS INTO THE THREE LINES. (1 + 2.7 + 4.3 = 8.0)
      SINTNS(1)=STOT*1./8.
      SINTNS(2)=STOT*2.7/8.
      SINTNS(3)=STOT*4.3/8.
D     TYPE*,'1',SINTNS,SMIN,SSLD,SMO,SAVG,STOT
C
C READ CONTROL DATA
  100       READ(6,*) TYP
C IF TYP=0, STOP.
      IF(TYP.NE.0)GOTO 1
      CLOSE(UNIT=1)
      CLOSE(UNIT=2)
      CLOSE(UNIT=3)
      CLOSE(UNIT=4)
      CLOSE(UNIT=6)
      CLOSE(UNIT=7)
      STOP
C
C
C IF TYP=1 SKIP TO GET NEW DENSITY, KEEP OLD TEMPERATURE.
    1       IF(TYP.EQ.1)GOTO 200
C GET NEW TEMPERATURE.
      READ(6,*) ABTMP
      TYPE*,'ABTMP=',ABTMP
C GET CROSS SECTION AND ATTENUATION DATA FOR
C THIS TEMPERATURE.
      IREC=(ABTMP/100.)-1
      READ(4'IREC) X1,ZIGMA
      READ(7'IREC) X1,ATTEN
C CALCULATE LINE CONSTANTS, ZGMA0.
      A=5.
      B=-228./ABTMP
      C=-326./ABTMP
      B=3.*EXP(B)
      C=EXP(C)
      CLC(1)=C/(A+B+C)
      CLC(2)=B/(A+B+C)
      CLC(3)=A/(A+B+C)
      ZGMA0=2.1E-13*SQRT(ETMP/ABTMP)
C
C LOOP HERE TO READ NEW DENSITIES.
  200       READ(6,*) OX
C
C NOW CALCULATE THE FLUX ABSORBED IN EACH SOURCE DISK, IN EACH
C OF THREE LINES.
      DO 7 JJ=1,3
C INITIAL ATTENUATION IS ONE.  DO SOME PRELIMINARY CALCULATIONS.
      AT2=1.
      POD=CLC(JJ)*OX*ZGMA0
D     TYPE*,'10',POD,CLC(JJ),OX,ZGMA0
C NOW FOR EACH SOURCE DISK, FIND THE OPTICAL DEPTH.
      DO 8 J=1,10
```

```
      OD=POD*(FLOAT(J)-.5)
C THE ATTENUATION DATA ONLY GOES UP TO OPTICAL DEPTHS OF 19.0.
      IF(OD.GT.19.0)OD=19.0
C USE THE INDEX INSTEAD OF OPTICAL DEPTH TO INTERPOLATE FOR THE
C ATTENUATION AT THIS POINT.
      IND=OD*2.+1.
      XIND=OD*2.+1.-FLOAT(IND)
      ATOUT=(ATTEN(IND+1)-ATTEN(IND))*XIND+ATTEN(IND)
D     TYPE*,'11',OD,IND,XIND,ATTEN(IND+1),ATTEN(IND)
C NOW THE FLUX
      FLUX(JJ,J)=(AT2-ATOUT)*SINTNS(JJ)
C SAVE THE ATTENUATION AND GO BACK.
D     TYPE*,'2',AT2,ATOUT,FLUX(JJ,J),SINTNS(JJ),AT2-ATOUT
      AT2=ATOUT
    8       CONTINUE
    7       CONTINUE
C
C NOW USING THESE 10 SOURCES, CALCULATE THE LIGHT TO THE DETECTOR
C DISKS THEN TO THE DETECTOR.
C READ RATIO AND VOLUME DATA, THEN SET FOR THE 3 LINES.
      READ(1'11) VOL
      READ(1'12) RAT
      TOTAL=0.
      DO 9 JJ=1,3
C PRELIMINARY OPTICAL DEPTH.
      POD=CLC(JJ)*OX*ZGMA0
C NOW FOR THE 10 SOURCES.  READ DISTANCES TO DETECTOR DISKS.
      TOT2=0.
      DO 10 I=1,10
      READ(1'I) DST
C FOR EACH DETECTOR DISK CALCULATE OPTICAL DEPTH TO DISK.
      TOT=0.
      DO 11 J=1,100
      OD=POD*DST(J)
C KEEP OPTICAL DEPTH IN RANGE.
      IF(OD.GT.19.0)OD=19.0
C USE INDEXES AND INTERPOLATE TO FIND THE EFFECTIVE CROSS SECTIONS.
      IND=OD*2.+1.
      XIND=OD*2.+1.-FLOAT(IND)
      XSECTN=(ZIGMA(IND+1)-ZIGMA(IND))*XIND+ZIGMA(IND)
C CALCULATE ABSORBER AREA TO TOTAL SPHERE, AND THEN THE LIGHT
C TO THE DETECTOR DISK.
      RATIO=((XSECTN*2.1E-13)*OX*VOL(J))/(4.*PI*DST(J)**2)
      SDSK=FLUX(JJ,I)*RATIO
C NOW MULTIPLY THE AMOUNT OF FLUX TO THE DISK BY THE DETECTOR
C AREA RATIO, TO GET FLUX TO THE DETECTOR, THEN ADD IT.
      TOT=TOT+SDSK*RAT(J)
D     TYPE*,'6',OD,XSECTN,RATIO,SDSK,FLUX(JJ,J),RAT(J)
C NOW GO DO THE NEXT DISK.
   11       CONTINUE
C KEEP TOTAL FOR THE SOURCES.
      TOT2=TOT2+TOT
   10       CONTINUE
```

```
C AND TOTAL FOR THE LINE.
     TOTAL=TOTAL+TOT2
     XLN(JJ)=TOT2
     9       CONTINUE
C DONE WITH THIS DENSITY-TEMPERATURE.
     WRITE(5,5) OX,XLN
     5       FORMAT(5X,E10.5,'  SUMS=',3F13.2)
     WRITE(3,*) ABTMP,OX,TOTAL,TOTAL/OX
     GOTO 100
     END
```

```
      PROGRAM ATOX
C
C ATOMIC OXYGEN MODELING PROGRAM.        J.K.ELWELL 7/13/79
C                                     REVISED 2/14/80  J.E.
C                                             REVISED 4/1/80   J.E.
C                                         REVISED 6/3/80   J.E.
C                                     REVISED 9/22/80  J.E.
C                                     REVISED 3/24/81  J.E.
C
C THIS GEOMETRY IS TO TEST THE NEW LAYOUT. 2/14/80
C
C NOW MODIFIED TO ACCEPT SPECIFICATIONS FOR ANY LAYOUT OF THE
C INSTRUMENT. 4/1/80
C
C PUT IN THE SUBROUTINE ANGLE TO FIND ANGLES, AND CHANGE TO
C INTERPOLATION TO FIND EFFECTIVE CROSS SECTION AND ATTENTUATION
C INSTEAD OF USING CURVE FITS.  6/3/80
C
C ALLOW FOR FOUR LETTER GEOMETRY SPECIFIER TO BE PUT IN THE
C ACTUAL FILE NAMES.  PROVIDE FOR THE PROPER CLOSING OF THE
C OPENED FILES.  9/22/80
C
C ALLOW FOR VARYING DENSITY VS. DISTANCE FROM ROCKET,
C I.E., WAKE EFFECTS.   3/24/81
C
C  STATEMENT OF VARIABLES:
C
C   ORIGIN  POINT LOCATED AT FIRST CONTACT OF DETECTOR AND SOURCE
 CONES
C
C   ABTMP   TEMPERATURE OF ABSORBING MEDIUM
C   AS      AREA OF SPHERE WITH RADIUS DR
C   ATOUT   ATTENUATION OUT FROM LIGHT TO OXYGEN
C   ATTEN   ARRAY GIVING ATTENUATION VS. OPTICAL DEPTH
C   CLC     CALCULATED LINE CONSTANTS
C   CNTRL   CONTROL DATA: 0=STOP,1=DENSITY,2=TEMPERATURE
C   DA      AREA OF DETECTOR
C   DAR     RADIUS OF DETECTOR APERTURE
C   DDB     DISTANCE FROM BACK POINT TO INTEGRATING ELEMENT
C   DD50    50/DMAX
C   DF      ARRAY GIVING AMOUNT OF OCCULTATION BY DETECTOR APERTURE
C   DINTNS  DETECTED INTENSITY
C   DMAX    DETECTOR CONE ANGLE AT OUTER EDGE OF OCCLUDED ZONE
C   DMIN    DETECTOR CONE ANGLE AT INNER EDGE OF OCCLUDED ZONE
C   DPHB    ANGLE AT BACK POINT FROM AXIS TO ELEMENT
C   DPHF    ANGLE AT FRONT POINT FROM AXIS TO ELEMENT
C   DR      RADIUS OF DETECTOR
C   DVB     Y DISTANCE FROM BACK POINT TO WHERE AXIS HITS Y AXIS
C   DVECB   LENGTH OF DETECTOR AXIS FROM BACK POINT TO Y AXIS
C   DVECF   LENGTH OF DETECTOR AXIS FROM FRONT POINT TO Y AXIS
C   DVF     Y DISTANCE FROM FRONT POINT TO WHERE AXIS HITS Y AXIS
C   DXB     X DISTANCE OF DETECTOR BACK POINT
C   DXF     X DISTANCE OF DETECTOR FRONT POINT
```

```
C   DYB      Y DISTANCE OF DETECTOR BACK POINT
C   DYF      Y DISTANCE OF DETECTOR FRONT POINT, ALWAYS =0
C   EANG     ANGLE AT WHICH EMITTER (LAMP) OUTPUT IS ZERO
C   EDIM     DIMMING FACTOR DUE TO BEING OFF EMITTER (LAMP) AXIS
C   EINTNS   EMITTER (LAMP) INTENSITY
C   ETMP     EMITTER (LAMP) TEMPERATURE
C   FLG1     FLAG USED TO INDICATE WHERE PROGRAM HAS BEEN
C   FLG2     FLAG USED TO INDICATE WHERE PROGRAM HAS BEEN
C   FOURPI   4*PI
C   GEO      INSTRUMENT GEOMETRY IDENTIFIER
C   IND      OPTICAL DEPTH INDEX
C   IREC     POINTS TO DIRECT ACCESS RECORDS
C   OD       OPTICAL DEPTH FROM LIGHT TO ELEMENT
C   OUT      MAXIMUM X DISTANCE TO INTEGRATE, IN CENTIMETERS
C   OX       DENSITY OF ATOMIC OXYGEN
C   PINTNS   PRELIMINARY INTENSITY
C   POD      PRELIMINARY OPTICAL DEPTH
C   SS       DISTANCE FROM SOURCE TO SOURCE APERTURE
C   SAR      SOURCE APERATURE RADIUS
C   SDB      DISTANCE FROM SOURCE BACK POINT TO INTEGRATING ELEMENT
C   SD50     50/SMAX
C   SF       ARRAY GIVING AMOUNT OCCULTATION AS A FUNCTION OF ANGLE
C   SIN      DISTANCE FROM SOURCE TO ROCKET SKIN
C   SINTNS   SOURCE INTENSITY FOR EACH LINE (PHOTONS/SEC-SR)
C   SMAX     SOURCE CONE ANGLE AT OUTER EDGE OF OCCLUDED ZONE
C   SMIN     SOURCE CONE ANGLE AT INNER EDGE OF OCCLUDED ZONE
C   SPHB     ANGLE AT BACK POINT FROM AXIS TO ELEMENT
C   SPHF     ANGLE AT FRONT POINT FROM AXIS TO ELEMENT
C   SR       RADIUS OF SOURCE
C   SRMI     DISTANCE FROM ROCKET SKIN TO INTEGRATING ELEMENT
C   SVB      Y DISTANCE FROM BACK POINT TO WHERE AXIS HITS Y AXIS
C   SVECB    LENGTH OF AXIS FROM BACK POINT TO Y AXIS
C   SVECF    LENGTH OF AXIS FROM FRONT POINT TO Y AXIS
C   SVF      Y DISTANCE FROM FRONT POINT TO WHERE AXIS HITS Y AXIS
C   SXB      X DISTANCE OF SOURCE BACK POINT
C   SXF      X DISTANCE OF SOURCE FRONT POINT
C   SYB      Y DISTANCE OF SOURCE BACK POINT
C   SYF      Y DISTANCE OF SOURCE FRONT POINT
C   VOL      VOLUME OF INTEGRATING ELEMENT
C   XIND     FRACTIONAL PART OF OPTICAL DEPTH INDEX
C   XSECTN   MICROSCOPIC CROSS SECTION
C   XX       INTEGRATION STEP SIZE IN X DIRECTION=2*ZTP
C   X*       X1,X2,X3,. . . .; DUMMY VARIABLES
C   ZGMA0    SIGMA0
C   ZIGMA    ARRAY GIVING EFFECTIVE CROSS SECTION VS. OPTICAL DEPTH
C   ZTP      INTEGRATION STEP SIZE, IN CENTIMETERS
C   ZTP0     INTIAL STEP SIZE FOR INTEGRATION
C   ZUM      PARTIAL SUM OF COUNTS
C   ZUMS     SUM OF COUNTS
C
C THIS PROGRAM SHOULD BE LINKED AS FOLLOWS:
C LINK/OPTIONS ATOX3,ANGLE,CNVFN
C MAXBUF=164
```

```
C UNITS=6
C ACTFIL=6
C /
C
C
      REAL SF(53),DF(53),CLC(3),ZIGMA(40),ATTEN(40),SINTNS(3)
      REAL PER,LNGTH,FRAC
      INTEGER FLG1,FLG2,CNTRL
      BYTE GEO(11)
C
      PARAMETER ETMP=900.,OUT=2000.,EANG=.5585,FOURPI=12.5664,DYF=0.
C
      DATA GEO/'D','S',4*0,'.','D','A','T',0/
C
C UNIT DEFINITIONS:
C     1-RUN CONTROL AND TEMPERATURE DATA
C     2-SPECIFICATIONS OF INSTRUMENT
C     3-OUTPUT CALCULATED RESULTS
C     4-CROSS SECTION VS. OPTICAL DEPTH DATA
C     5-TERMINAL
C     6-ATTENUATION VS. OPTICAL DEPTH DATA
C
      TYPE*,'ENTER THE FOUR LETTER GEOMETRY IDENTIFIER.'
      ACCEPT6, (GEO(K),K=3,6)
      6       FORMAT(4A1)
C
      OPEN(UNIT=1,NAME='DINDAT.DAT',TYPE='OLD')
      OPEN(UNIT=2,NAME=GEO,TYPE='OLD')
      GEO(2)='1'
      OPEN(UNIT=3,NAME=GEO,TYPE='NEW')
      OPEN(UNIT=4,NAME='DSIGMA.DAT',TYPE='OLD',ACCESS='DIRECT')
      OPEN(UNIT=6,NAME='DB0:DATTEN.DAT',TYPE='OLD',ACCESS='DIRECT')
C
C
C THE FOLLOWING SPECIFICATIONS COMPLETELY DEFINE
C THE GEOMETRY OF THE INSTRUMENT.
      READ(2,*) SR,SAR,SS,SIN
      READ(2,*) SXB,SYB,SXF,SYF
      READ(2,*) SVECB,SVECF,SVB,SVF
      READ(2,*) DR,DAR,DS,X1
      READ(2,*) DXB,DYB,DXF,X1
      READ(2,*) DVECB,DVECF,DVB,DVF
      READ(2,*) X1,X2,X3
C
C NOW CALCULATE THE AREA OF THE DETECTOR, AND CONSTANTS.
      DA=3.1416*DR**2
C
      SMIN=ATAN((SAR-SR)/SS)
      SMAX=ATAN((SAR+SR)/SS)
      SD50=50./SMAX
C
      DMIN=ATAN((DAR-DR)/DS)
      DMAX=ATAN((DAR+DR)/DS)
```

```
      DD50=50./DMAX
C
C ASSUME SOURCE INTENSITY OF 1.E13 PHOTONS/SEC-SR
C LINE INTENSITY RATIOS OF 1:2.7:4.3
      SINTNS(1)=1.25E12
      SINTNS(2)=3.375E12
      SINTNS(3)=5.375E12
C
      TYPE*,'ENTER INITIAL INCREMENT SIZE.'
      ACCEPT*,ZTP0
      TYPE*,' '
C
C GET PERCENTAGE CHANGE AND DISTANCE OUT AFFECTED
C BY WAKE EFFECTS.
      TYPE*,'ENTER PERCENT CHANGE AND LENGTH AFFECTED BY WAKE.'
      ACCEPT*,PER,LNGTH
C
C FIND CONVOLUTION OF PROJECTED APERTURE AND SOURCE OR DETECTOR AREA.
      CALL CNVFN(SR,SAR,SS,SMIN,SMAX,SF)
      CALL CNVFN(DR,DAR,DS,DMIN,DMAX,DF)
C
C READ CONTROL DATA
  100       READ(1,*) CNTRL
C IF TYP=0, STOP.
      IF(CNTRL.NE.0)GOTO 7
      CLOSE(UNIT=1)
      CLOSE(UNIT=2)
      CLOSE(UNIT=3)
      CLOSE(UNIT=4)
      CLOSE(UNIT=6)
      STOP
C
C
C IF TYP=1 SKIP TO GET NEW DENSITY, KEEP OLD TEMPERATURE.
    7       IF(CNTRL.EQ.1)GOTO 200
C GET NEW TEMPERATURE.
      READ(1,*) ABTMP
      TYPE*,'ABTMP=',ABTMP
C GET CROSS SECTION AND ATTENUATION DATA FOR
C THIS TEMPERATURE.
      IREC=(ABTMP/100.)-1
      READ(4'IREC) X1,ZIGMA
      READ(6'IREC) X1,ATTEN
C CALCULATE LINE CONSTANTS, ZGMA0.
      A=5.
      B=-228./ABTMP
      C=-326./ABTMP
      B=3.*EXP(B)
      C=EXP(C)
      CLC(1)=C/(A+B+C)
      CLC(2)=B/(A+B+C)
      CLC(3)=A/(A+B+C)
      ZGMA0=2.1E-13*SQRT(ETMP/ABTMP)
```

```
C
C LOOP HERE TO READ NEW DENSITIES.
  200       READ(1,*) OX
C
C ** ONE TIME FOR EACH LINE **
    ZUMS=0.
    DO 10 JJ=1,3
C CALCULATE SOME PRELIMINARY NUMBERS.
    POD=CLC(JJ)*ZGMA0
    PINTNS=SINTNS(JJ)*OX*CLC(JJ)
C CLEAR SUM, SET INITIAL INCREMENTS.
    ZUM=0.
    ZTP=ZTP0
C THE INCREMENT SIZE IN THE X DIRECTION IS TWICE THE
C SIZE OF THE INCREMENT IN THE Y AND Z DIRECTION.
    XX=2.*ZTP0
C BY NOT SETTING X BACK ONE FULL INCREMENT, AFTER THE FIRST
C INCREMENT OPERATION THE INTEGRATION STARTS SLIGHTLY INSIDE
C THE VOLUME, ELIMINATING MANY BORDER PROBLEMS.
    X=-4./5.*XX
C SET INITIAL DIFFERENTIAL VOLUME.
    VOL=ZTP**2*XX
    Y=0.
C
C
C WE NOW ENTER THE INTEGRATING LOOPS: X,Y,Z.
C
C
C************ THE X LOOP ***************
C
C CHECK TO SEE IF VOL AND ZTP NEED RESCALING. IF NOT THEN BRANCH.
    1       IF(ZTP.GT.Y/20.)GOTO 20
C KEEP THE STEP SIZE BETWEEN 10 AND 20 TIMES THE
C WIDTH OF THE INTERSECTION OF THE SOURCE AND DETECTOR
C CONES AT THE PRESENT DISTANCE OUT.
    ZTP=Y/10.
    XX=2.*ZTP
    VOL=ZTP**2*XX
C*** NOW START THE ACTUAL LOOP ***
   20       X=X+XX
C
C LEAVE IF WE HAVE REACHED THE END.
C THIS IS FOR GEOMETRIES WITH INFINITE VOLUMES.
    IF(X.GT.OUT)GOTO 40
    FLG1=0
    Y=-ZTP
C
C************ THE Y LOOP ***************
C
    2       Y=Y+ZTP
    FLG2=0
    Z=-ZTP
C
```

```
C************ THE Z LOOP ***************
C
    3       Z=Z+ZTP
C
C NOW FIND IF THE POINT(X,Y,Z) IS IN BOTH CONES.  THE ANGLE
C TO THIS POINT IS MEASURED FROM THE FRONT POINT OF THE
C DETECTOR OR SOURCE.
C
C CALL ANGLE TO FIND ANGLE BETWEEN INTEGRATING ELEMENT AND
C THE SOURCE CONE AXIS.
    CALL ANGLE(X,Y,Z,SXF,SYF,SVF,SVECF,X1,SPHF)
C IF THE ANGLE IS TOO GREAT, LEAVE.
    IF(SPHF.GT.SMAX)GOTO 30
C
C NOW DO THE SAME FOR THE DETECTOR CONE.
    CALL ANGLE(X,Y,Z,DXF,DYF,DVF,DVECF,X1,DPHF)
C IF ANGLE IS TOO GREAT, LEAVE.
    IF(DPHF.GT.DMAX)GOTO 30
C
C WE HAVE A GOOD POINT!!!!!
C
C NOW FIND ANGLE FOR SOURCE OCCLUSION, WHICH IS THE ANGLE
C SEEN FROM THE BACK POINT.
    CALL ANGLE(X,Y,Z,SXB,SYB,SVB,SVECB,SDB,SPHB)
C AND FOR THE DETECTOR OCCLUSION.
    CALL ANGLE(X,Y,Z,DXB,DYB,DVB,DVECB,DDB,DPHB)
C
C
C SUBTRACT DISTANCE INSIDE OF ROCKET.
    SRMI=SDB-SIN
C NOW WE PROCESS THE INTEGRATING VOLUME AND FIND THE COUNTS.
C
C FIND THE AMOUNT OF OCCLUSION AT THIS ANGLE.
    I=SPHB*SD50+1.5
    J=DPHB*DD50+1.5
    FS=SF(I)
    FD=DF(J)
C NOW THE REAL CALCULATIONS.
C THE ATTENUATION AND CROSS SECTION DATA ONLY GO UP TO
C AN OPTICAL DEPTH OF 19.5, SO IF THE ACTUAL OPTICAL DEPTH
C IS GREATER THAN THIS, MAKE IT EQUAL TO 19.5.
C
C CALCULATE THE EFFECT OF WAKE AT THIS POINT.
    IF(SRMI.LT.LNGTH)GOTO 50
    FRAC=1.
    GOTO 51
   50       FRAC=(LNGTH-SRMI)/LNGTH*PER+1.
   51       OD=POD*SRMI*OX*FRAC
    IF(OD.GT.19.5)OD=19.5
C USING THE OPTICAL DEPTH, INTERPOLATE IN BOTH ZIGMA
C AND ATTEN TO FIND THE ACTUAL ATTENUATION AND CROSS SECTION.
C FIRST, USE INDEXES INSTEAD OF OPTICAL DEPTH TO INTERPOLATE.
    IND=OD*2.+1.
```

```
      XIND=OD*2.+1.-FLOAT(IND)
      XSECTN=(ZIGMA(IND+1)-ZIGMA(IND))*XIND+ZIGMA(IND)
      ATOUT=(ATTEN(IND+1)-ATTEN(IND))*XIND+ATTEN(IND)
C
      EINTNS=PINTNS*VOL*(XSECTN*2.1E-13)/(SDB**2)
C EDIM IS THE DIMMING OF LIGHT FROM THE SOURCE AT THIS ANGLE.
      EDIM=(EANG-SPHB)/EANG
      EINTNS=FS*EINTNS*ATOUT*EDIM
      AS=FOURPI*DDB**2
      DINTNS=EINTNS*FD*(DA/AS)
C DINTNS IS NOW THE COUNTS/SEC FROM THIS INTEGRATING VOLUME.
      ZUM=ZUM+2.*DINTNS
C NOW SET FLAGS TO INDICATE WHERE WE HAVE BEEN.
      FLG1=1
      FLG2=1
C LET'S GO BACK AND DO ANOTHER PIECE IN THE Z DIRECTION.
      GOTO 3
C
C******* END OF Z LOOP **********
C
C NOW FIND OUT WHY WE ARE OUT OF THE CONES.
C
C IF FLG1=0 WE HAVE NOT FOUND ANY DATA AT THIS X VALUE, SO WE
C ARE DONE WITH THIS LINE.
   30       IF(FLG1.EQ.0)GOTO 40
C
C IF FLG1=1 AND FLG2=1 WE GOT TOO FAR UP ON THE Z AXIS, SO GO RESET
C Z AND MOVE FARTHER OUT ON THE Y AXIS.
      IF(FLG1.EQ.1.AND.FLG2.EQ.1)GOTO 2
C
C SINCE FLG1=1 AND FLG2=0, WE RAN OUT OF GOOD SPACE AT THIS X VALUE.
C GO BACK AND MOVE ALONG THE X AXIS.
      GOTO 1
C
C******* END OF INTEGRATION LOOPS ********
C
C WE ARE DONE!!!!!!
C
   40       ZUMS=ZUMS+ZUM
   10       CONTINUE
      WRITE(5,5) OX,ZUMS,ZUMS/OX
5     FORMAT(5X'OX=',E10.5,'  SUMS=',F13.2,'  RATIO=',E10.5)
      WRITE(3,*) ABTMP,OX,ZUMS,ZUMS/OX
      GOTO 100
C
      END
```

```
      PROGRAM PLOTT
C
C THIS PROGRAM PLOTS THE ATOMIC OXYGEN MODEL RESULTS FOR A
C GIVEN INSTRUMENT GEOMETRY, AND CREATES A FILE WITH THE SUM OF
C THE FIRST AND SECOND ORDER SCATTERING.
C                                  J.K.ELWELL      6/5/80
C
C      REVISED 9/22/80      J.ELWELL
C
C LINK AS FOLLOWS:
C LINK/OPTIONS PLOTT,[245,1]LOGAX,[7,7]MAPPED,[7,7]PEPLIB/LIB
C UNITS=10
C ACTFIL=10
C /
C
C   STATEMENT OF VARIABLES
C
C   ABTMP   TEMPERATURE OF ABSORBER
C   AB2     OLD TEMPERATURE
C   FLG     FLAG
C   FST     FIRST ORDER SCATTERING DATA
C   GEO     INSTRUMENT GEOMETRY IDENTIFIER
C   GEO2    INSTRUMENT GEOMETRY IDENTIFIER
C   OX      OXYGEN DENSITY
C   RAT     RATIO OF DENSITY TO COUNTS
C   SND     SECOND ORDER SCATTERING DATA
C   TMP     ATOMIC OXYGEN TEMPERATURE
C   TOT     FST+SND
C   X       X COORDINATE ON PLOTS
C   Y       Y COORDINATE ON PLOTS
C
C
      REAL OX(20),TOT(20),ABTMP,AB2,RAT
      BYTE GEO(15),GEO2(4),FLG
C
      EQUIVALENCE (GEO(7),GEO2(1))
C
      DATA GEO/'D','B','0',':','D','1',4*0,'.','D','A','T',0/
C
C UNIT DEFINITIONS:
C   1-4:  USED BY PLOTTING ROUTINES
C   5:  TERMINAL
C   6:  FIRST ORDER SCATTERING DATA
C   7:  SECOND ORDER SCATTERING DATA
C   10:  OUTPUT
C
C GET GEOMETRY IDENTIFIER AND OPEN FILES.
      TYPE*,'ENTER THE FOUR CHARACTER GEOMETRY IDENTIFIER.'
      ACCEPT1,GEO2
      1       FORMAT(4A1)
C OPEN FILES.
      OPEN(UNIT=6,NAME=GEO,TYPE='OLD')
      GEO(6)='2'
```

```
      OPEN(UNIT=7,NAME=GEO,TYPE='OLD')
      GEO(6)='F'
      OPEN(UNIT=10,NAME=GEO,TYPE='NEW',ACCESS='DIRECT',RECORDSIZE=16)
C
C PREPARE FOR PLOTTING AND PUT ON THE TITLE PAGE.
      CALL PLOTS(0,0,0)
      CALL SYMBOL(2.,2.625,.25,'ATOX MODEL RESPONSE',90.,+19)
      CALL SYMBOL(3.,1.625,.15,'INSTRUMENT COUNT RATE VS ATOM
     +IC OXYGEN DENSITY',90.,+46)
      CALL SYMBOL(3.5,2.45,.15,'FOR INCREASING OXYGEN TEMPERATURES'
     +,90.,+34)
      CALL SYMBOL(4.5,3.50,.15,'INSTRUMENT GEOMETRY:',90.,+20)
      CALL NEWPEN(5)
      CALL SYMBOL(5.9,3.0,1.,GEO2,90.,+4)
      CALL NEWPEN(1)
      CALL PLOT(0.,0.,-999)
C
C NOW DO 9 PLOTS FOR 9 TEMPERATURES, AND READ IN THE 8 DENSITIES
C FOR EACH TEMP.
      FLG=1
      DO 9 J=1,100
      DO 8 K=1,100
      READ(6,*,END=33) ABTMP,OX(K),FST,RAT
      READ(7,*,END=33) ABTMP,OX(K),SND,RAT
      TOT(K)=FST+SND
      IF(FLG.NE.1)GOTO 37
C THIS IS FIRST TIME AT THIS TEMPERATURE
      FLG=0
      AB2=ABTMP
C NOW SEE IF A NEW TEMPERATURE HAS BEEN READ
   37       IF(AB2.NE.ABTMP)GOTO 34
C NO NEW TEMPERATURE, SO JUST CONTINUE READING
    8       CONTINUE
C HERE WHEN END OF FILE HAS BEEN REACHED
   33       FLG=2
      GOTO 36
C HERE WHEN NEW TEMP HAS BEEN REACHED, SO PROCESS OLD ONE
   34       FLG=1
      BACKSPACE 6
      BACKSPACE 7
C GET NUMBER OF DENSITIES AT THIS TEMPERATURE
   36       NUM=K-1
C WRITE THIS TEMP DATA TO THE FINAL DATA FILE.
      WRITE(10'J) (OX(I),TOT(I),I=1,NUM)
      TYPE*,'TOT',(OX(I),TOT(I),I=1,NUM)
C NOW FIND THE TEMPERATURE, MOVE THE ORIGIN AND PLOT AXIS AND LABELS.
      CALL PLOT(7.2,1.,-3)
      CALL LOGAX(0.,0.,7,7.,6.,'[OX]',90.,-4)
      CALL LOGAX(0.,0.,7,7.,1.,'COUNTS PER SECOND',180.,+17)
      CALL SYMBOL(-1.,7.5,.1,'TEMPERATURE:',90.,+12)
      CALL NUMBER(-.6,7.8,.2,AB2,90.,-1)
      CALL SYMBOL(-.6,8.6,.2,'K',90.,+1)
      CALL SYMBOL(-2.9,7.65,.1,'GEOMETRY:',90.,+9)
```

```
      CALL SYMBOL(-2.6,7.9,.2,GEO2,90.,+4)
C NOW PLOT THE 8 POINTS FOR THIS TEMPERATURE.
      DO 10 K=1,NUM
      X=ALOG10(OX(K))-6.
      Y=-(ALOG10(TOT(K))-1.)
      CALL SYMBOL(Y,X,.08,46,90.,-1)
   10       CONTINUE
C DONE WITH THIS PAGE.
      CALL PLOT(0.,0.,-999)
      IF(FLG.EQ.2)GOTO 35
      9        CONTINUE
C DONE.
   35       CALL PLOT(0.,0.,+999)
      CLOSE(UNIT=6)
      CLOSE(UNIT=7)
      CLOSE(UNIT=10)
      STOP'THE VERY END'
      END
```

```
      PROGRAM FINAL
C
C
C ******************* FINALTR.FTN ***************************
C
C    FINAL REDUCTION FOR 'TRACER'      7/20/82  NEIL MYERS
C
C         UPLEG ONLY.....
C
C   ERROR BARS COMPUTED IN THIS PROGRAM.
C                        8/9/82     NEIL MYERS
C
C
C
C    TRACER TEMP. PROFILE INSERTED 5/26/83  Neil Myers
C
C
C     MEASURED LAMP INTENSITY MONITOR INSERTED 7/26/82  NEIL MYERS
C
C
C
C
C
C THIS PROGRAM CALCULATES THE FINAL COUNT RATES AND DENSITIES,
C BY AVERAGING OVER A SPECIFIED TIME OR SPACE BLOCK.
C                    REVISED 12/28/80   J.ELWELL
C
C
C
C
C       TO LINK:
C               LINK/OPTIONS FINALTR
C       OPTIONS?ACTFIL=6
C       OPTIONS?UNITS=6
C       OPTIONS?/
C
C
C
      COMMON TIM,CNTS,TMP,ALT,OX,SD
      COMMON /A/TYP,SPD,TT1,T2,T3,R2,ATT
      INTEGER ID,TYP,R2
      REAL TIM,TT1,T2,T3
      REAL TMP,CNTS,ALT,OX,RA,ATT,SPD,RNG
C
C PARAMETERS FOR A SPECIFIC INSTRUMENT AND FLIGHT.
C  STRTTM IS TIME OF FIRST SAMPLE
C  STRALT IS ALTITUDE OF FIRST SAMPLE
C  FACTOR IS THE GEOMETRICAL EFFECIENCY FACTOR
C
C  THESE PARAMATERS ARE FOR THE 'TRACER' ROCKET FLIGHT.
C                                              7/20/82  NEIL MYERS
C
      PARAMETER STRTTM=43.5136,STRALT=40.0080,FACTOR=53360.
```

```
C
C
      OPEN(UNIT=1,NAME='TRADIR.DAT',TYPE='OLD',ACCESS='DIRECT')
      OPEN(UNIT=2,NAME='DFGE06.DAT',TYPE='OLD',ACCESS='DIRECT')
      OPEN(UNIT=3,NAME='OUTTR.DAT',TYPE='NEW',ACCESS='DIRECT'
     +,RECORDSIZE=3)
      OPEN(UNIT=4,NAME='ERBRTR.DAT',TYPE='NEW')
C
C NOW FIND AVERAGE AND TIME OF DATA
      ID=1
      II=0
C
      TYPE*,'1-TIME AVERAGE, 2-SPACE AVERAGE.'
      ACCEPT*,TYP
      TYPE*,'HOW OFTEN (KM OR SECS)?'
      ACCEPT*,SPD
      TYPE*,'HOW MUCH (KM OR SECS)?'
      ACCEPT*,RNG
      WRITE(3'1) TYP,SPD,RNG
      WRITE(4,222)TYP,SPD,RNG
  222   FORMAT(1X,I1,2F6.2)
      R2=0
      IF(TYP.EQ.2)GOTO 3
C SET UP INITIAL VALUES.
      TT1=STRTTM
      T2=STRTTM+RNG/2.-SPD
      T3=STRTTM+RNG-SPD
      GOTO 10
3     TT1=STRALT
      T2=STRALT+RNG/2.-SPD
      T3=STRALT+RNG-SPD
      ATT=0
C NOW CALL AVRGE TO DO THE AVERAGING.
10    CALL AVRGE(II)
      IF(II.EQ.-1)GOTO 300
C
C MULTIPLY BY 1/(16 MSECS)*(?:GEOMETRICAL FACTOR)
      CNTS=CNTS*FACTOR
C
C NOW FIND HEIGHT, TEMPERATURE, AND DENSITY
      IF(CNTS.LT.0.)TYPE*,'NEGATIVE AVERAGE FOUND.'
      IF(CNTS.EQ.0.)OX=0.
      IF(CNTS.LE.0.)GOTO 10
      CALL TERP(RA)
C
C WRITE RESULTS.
      TYPE*,TIM,ALT,CNTS,OX,SD
      ID=ID+1
      WRITE(3'ID) ALT,CNTS,OX
          WRITE(4,333)ALT,SD
  333     FORMAT(1X,F10.5,F10.5)
          IF(ALT.GT.130.)GOTO 300
          IF(ALT.GE.40.)GOTO 10
```

```
C
  300       TYPE*,'RECORDS=',ID
    CLOSE(UNIT=1)
    CLOSE(UNIT=2)
    CLOSE(UNIT=3)
    CLOSE(UNIT=4)
    STOP'THE VERY END'
    END
C
    SUBROUTINE TERP(RA)
    COMMON TIM,CNTS,TMP,ALT,OX
    INTEGER INT,IND
    REAL CNTS,TMP,ALT,TEMP(81),TMO,OX,C1(8),C2(8),OX1,OX2,TIM
    REAL DY,DNS(8),VOLT(33),RA,DUMMY(8)
C
C CAL IS THE VOLTAGE OF THE INTENSITY MONITOR DURING CALIBRATION.
C
    PARAMETER CAL=3.6
    DATA DNS/1.E7,1.E9,1.E10,1.E11,3.33E11,1.E12,3.33E12,1.E13/
C
C TEMP HOLDS THE TEMPERATURE FOR ALTITUDES FROM 60 TO
C 140 KM, IN 1 KM INCREMENTS.
C
       DATA TEMP/230.,230.,230.,229.2,226.6,218.3,218.3,208.2,
     +200.5,194.1,193.8,192.5,186.1,183.4,181.4,184.2,183.1,184.7,
     +190.5,211.9,213.5,204.1,193.4,184.4,168.7,164.4,163.1,177.5,
     +174.9,175.3,171.7,171.3,171.,172.7,163.6,160.9,172.9,173.5,
     +165.7,160.7,157.1,154.,156.,166.9,208.2,231.9,255.7,278.1,
     +298.7,310.1,310.5,305.8,302.2,302.9,307.5,316.4,330.5,349.6,
     +373.5,400.2,427.,453.9,478.8,502.7,526.3,546.4,561.6,567.5,
     +571.1,576.6,588.4,603.2,610.5,603.8,586.8,576.1,586.1,611.3,
     +635.1,633.9,612./
C
C VOLT HOLDS THE DATA FROM THE INTENSITY MONITOR, STARTING AT 40 SECS,
C IN 5 SECOND INCREMENTS.
       DATA VOLT/1.,1.,1.2,1.55,2.,2.25,2.15,2.,1.9,1.75,1.6,1.45,
     +1.3,1.25,.95,.85,.8,.8,.65,.3,.6,.6,.4,.4,.1,.6,.4,.4,.25,.5,
     +.1,.3,.1/
C
C
C NOW INTERPOLATE TO FIND TEMPERATURE.
    INT=(ALT-60)+1
    FRAC=(ALT-59.-FLOAT(INT))
    TMP=TEMP(INT)+FRAC*(TEMP(INT+1)-TEMP(INT))
    IF(TMP.LT.200.)TMP=200.
C
C NOW INTERPOLATE TO GET INTENSITY CHANGES.
    INT=(TIM-40.)/5.+1
    FRAC=(TIM-35.-INT*5.)/5.
    VLT=VOLT(INT)+FRAC*(VOLT(INT+1)-VOLT(INT))
    CNTS=CNTS*CAL/VLT
C
C NOW INTERPOLATE TO GET DENSITY.
```

```
      IND=TMP/100-1
      READ(2'IND) (DUMMY(KK),C1(KK),KK=1,8)
      READ(2'IND+1) (DUMMY(KK),C2(KK),KK=1,8)
      DO 9 I=1,8
      IF(C1(I).GT.CNTS) GOTO 10
9     CONTINUE
      OX=-1
      RETURN
C
10    I=I-1
      DY=DNS(I+1)-DNS(I)
      OX1=DY/ABS(C1(I+1)-C1(I))*(CNTS-C1(I))+DNS(I)
      OX2=DY/ABS(C2(I+1)-C2(I))*(CNTS-C2(I))+DNS(I)
      OX=OX1+ABS(OX2-OX1)/100.*(TMP-100.*(IND+1))
      RETURN
      END
      SUBROUTINE AVRGE(II)
      COMMON /A/TYP,SPD,TT1,T2,T3,R2,ATT
      COMMON TIM,CNTS,TMP,ALT,OX,SD
      INTEGER TYP,R1,R2,FLG1,FLG2,FLG3,IX
      REAL TIM,TM,T2,T3,TT1
      REAL CNTS,TMP,ALT,OX,AT,AT1,SPD,ATT
C
C TWOMAX IS TWICE THE MAXIMUM ALTITUDE OF THE ROCKET.
C
      PARAMETER TWOMAX=296.7476
C
      IX=0
          X2=0.
      SUM=0
      FLG1=0
      FLG2=0
      FLG3=0
      T2=T2+SPD
      T3=T3+SPD
      TT1=TT1+SPD
      R1=R2
      AT1=ATT
C
      IF(TYP.EQ.2)GOTO 70
C
10    R1=R1+1
      READ(1'R1,ERR=300) TM,AT,ION,IOFF,DAT
          IF(AT.GT.130.)GOTO 300
          IF(AT.LT.60.)GOTO 10
C THIS NEXT IS TO CATCH THE FIRST RECORD WHICH IS IN THE NEXT FRAME
      IF(TM.LE.TT1.OR.FLG1.NE.0)GOTO 6
      R2=R1-1
      FLG1=1
C THIS NEXT IS TO CACHT THE MIDDLE OF THE PRESENT FRAME.
6     IF(TM.LT.T2.OR.FLG2.NE.0)GOTO 7
      TIM=TM
      ALT=AT
```

```
      FLG2=1
C BRANCH AT END OF THIS FRAME; OTHERWISE ADD COUNTS.
7     IF(TM.GT.T3.OR.TM.LT.TT1-SPD)GOTO 8
      IX=IX+1
      SUM=SUM+DAT
      GOTO 10
C NOW BRANCH IF SOMETHING WAS FOUND.
8     IF(IX.GT.0)GOTO 9
      CNTS=-1
      RETURN
9     CNTS=SUM/FLOAT(IX)
      IF(FLG1.EQ.0)R2=R1
      RETURN
C
C
70    R1=R1+1
      READ(1'R1,ERR=300) TM,AT,ION,IOFF,DAT
          IF(AT.GT.130.)GOTO 300
      IF(AT.LT.60.)GOTO 70
      IF(AT.LT.AT1)FLG1=1
      AT1=AT
      IF(FLG1.EQ.1)AT1=TWOMAX-AT
      IF(AT1.LE.TT1.OR.FLG2.NE.0)GOTO 76
      R2=R1-1
      ATT=AT1
      FLG2=1
76    IF(AT1.LT.T2.OR.FLG3.NE.0)GOTO 77
      TIM=TM
      ALT=AT
      FLG3=1
77    IF(AT1.GT.T3)GOTO 78
      IX=IX+1
      SUM=SUM+DAT
          X2=X2+DAT**2
      GOTO 70
78    IF(IX.GT.0)GOTO 79
      CNTS=-1
      RETURN
79    CNTS=SUM/FLOAT(IX)
          A=FLOAT(IX)
          SD2=(ABS(A*X2-SUM**2))/(A*(A-1))
          SD=SQRT(SD2)
      RETURN
C
300   II=-1
      RETURN
      END
```